MAGNETIC AND HIGH PRESSURE STUDIES IN THE $YPd_5B_3C_{.3}$ SYSTEM

By

Jim Murdoch

B. Sc. (Physics) Brock University

A THESIS SUBMITTED IN PARTIAL FULFILLMENT OF

THE REQUIREMENTS FOR THE DEGREE OF

MASTER OF SCIENCE

in

THE FACULTY OF MATHEMATICS AND SCIENCE

DEPARTMENT OF PHYSICS

We accept this thesis as conforming

to the required standard

.....

.....

.....

.....

.....

BROCK UNIVERSITY

August 1995

In presenting this thesis in partial fulfilment of the requirements for an advanced degree at Brock University, I agree that the Library shall make it freely available for reference and study. I further agree that permission for extensive copying of this thesis for scholarly purposes may be granted by the head of my department or by his or her representatives. It is understood that copying or publication of this thesis for financial gain shall not be allowed without my written permission.

Department of Physics
Brock University
500 Glenridge Avenue
St. Catharines, Ontario
Canada L2S 3A1

Date:

Abstract

The macroscopic properties of the superconducting phase in the multiphase compound $YPd_5B_3C_{.3}$ have been investigated. The onset of superconductivity was observed at 22.6 K, zero resistance at 21.2 K, the lower critical field H_{c1} at 5 K was determined to be $H_{c1}(5) \sim 310$ Gauss and the compound was found to be an extreme type-II superconductor with the upper critical field in excess of 55000 Gauss at 15 K.

From the upper and lower critical field values obtained, several important parameters of the superconducting state were determined at T = 15 K. The Ginzburg-Landau paramater was determined to be $\kappa > 9$ corresponding to a coherence length $\xi \sim 80\mathring{A}$ and magnetic penetration depth of $800\mathring{A}$.

In addition measurements of the superconducting transition temperature $T_c(P)$ under purely hydrostatically applied pressure have been carried out. $T_c(P)$ of $YPd_5B_3C_{.3}$ decreases linearly with $dT_c/dP \sim -8.814 \times 10^{-5} K/bar$. The discussion of $T_c(P)$ will focus on the influence pressure has on the phonon spectrum and the density of states near the Fermi level.

Table of Contents

List of Tables

List of Figures

Acknowledgement

I would like to take the time to express my appreciation to my supervisor, Dr. F.S. Razavi, for taking on the monumental task of having me as a graduate student. Your support and encouragement over the last two years are greatly appreciated but more importantly I thank you for your patience.

A very special thanks goes to Dr. B. *Mitrović* for the countless discussions we had regarding aspects of this thesis. Your invaluable advice and insight as well as your impeccable choice of football teams (**Go Raiders**) will not be forgotten.

I am also grateful to other members of the department. Dr. G. Quirion for his assistance in the laboratory with my experimental apparatus and for the many answered questions. I wish to thank Dr. M. Reedyk for taking the time to proof read the thesis and for offering her advice to help solve problems when I encountered them.

To my friends in the department I thank you for putting up with me during our years, as difficult as it must have been. To Elvis, Steffer, Zeke, Bunsen Honeydew, Katarin, Rob , the Boy Scout Ron Snelgrove and even you Smevil (What have you done for me lately?), I wish you continued success in your future endeavors. To Frank Benko, may you now enjoy your daily tea and coffee free of unwanted and often fouling tasting additives that some how found your cup.

Finally and most importantly I thank Tatiana. Words alone are incapable of expressing my gratitude. Three years ago I never would have considered graduate studies yet here I am about to complete them thanks to you. Never has any person given so much and asked for nothing in return. I love you.

Dedicated to the memory of my Grandfather, James Rae Murdoch, who passed away September 4, 1994. You left so suddenly that I didn't have a chance to say good-bye.

Chapter 1

Introduction

This was the greatest disturbance in the history of Hellenes,
affecting also a large part of the non-Hellenic world, and indeed,
I might say, the whole of mankind.

Thucydides, "History of the Peloponnesian War"

Although the fascinating phenomenon of superconductivity has been known for 80 years, it is largely through concentrated experimentation in the last decade that interest has been propelled to its current heights. In April 1986, two researchers at IBM in Switzerland, Alex *Müller* and George Bednorz, detected superconductivity in $(La-Ba)_2CuO_4$ with a $T_c \approx 35K$ [1]. By the end of 1986, superconductivity research achieved revolutionary advances with the effort of Paul C. W. Chu and colleagues at the University of Houston [2]. Signs of superconductivity above 77 K were repeatedly observed in poorly-characterized samples during the period, strongly affirming the belief in the existence of superconductivity in the liquid-nitrogen temperature range. The scientific world knew that textbooks had to be rewritten after January 1987, when the Houston group in collaboration with M.K. Wu, then at the University of Alabama at Huntsville, achieved stable and reproducible superconductivity above 90 K in $YBa_2Cu_3O_7$, with T_c close to 100 K [3].

In addition to the savings in cost resulting from the displacement of liquid helium by liquid nitrogen for cooling, it is now apparent that superconductivity applications

with more inexpensive refrigerants – or eventually no refrigerant at all – are possible. The race for new superconductors with higher T_c continues. Bismuth and Thallium superconducting systems were discovered in 1988 [4]which superconduct at 110 K and 125 K, respectively. The mercury-based compounds were discovered in 1993 [5], with temperatures up to 164 K under pressure. Many laboratories throughout the world have reported glimpses of superconductivity at much higher temperatures but these have not yet been confirmed.

It has widely been speculated that the low mass of boron should be conducive to the occurrence of high phonon frequency [6] and consequently high T_c's, and indeed many boride superconductors are known. Generally, however, these have low T_c's in the 2-7 K range [7]. The highest T_c previously reported for intermetallic borides was 11.7 K for $LuRh_4B_4$, and more recently at 12 K in samples of yttrium nickel boride [8]. The discovery of superconductivity in a new family of boron-carbide intermetallics, Y-Pd-B-C ($T_c \approx 23.2K$) by the Cava group [9] in January of 1994 again raised the question about how many roads can lead to a high T_c. This superconducting transition temperature matches the record T_c observed in the intermetallic compound Nb_3Ge in 1973. As well as having relatively high T_c's these intermetallic compounds appear to be chemically more stable than cuprate high temperature superconductors. Since they are non-oxides, more practical metals, such as copper, are compatible with them for wire processing. Soon after the discovery by Cava et al, a group at the Department of Physics and Texas Centre for Superconductivity at the University of Houston lead by Xue [10] investigated the macroscopic magnetic properties of the multiphased $YPd_5B_3C_{.3}$ and reported that the compound was an extreme type II superconductor with upper critical field H_{c2} at 0 K, $H_{c2}(0) \approx 9$ T[1] and a Ginzburg– Landau parameter $\kappa > 10$. It appeared the race was underway to discover new boride compounds with even higher T_c's. The next group

[1] 1T = 10^4 Gauss

to report results on the Y-Pd-B-C system was H.W. Zandbergen [11] at the National Centre for HREM [2]. Here superconducting and non–superconducting specimens were investigated with electron diffraction, electron dispersive x-ray analysis and HREM. Here it was reported that $YPd_5B_3C_{.3}$ contains six different phases , of which four are crystalline. It was suggested by this group that the phase responsible for superconductivity was YPd_2B_2C because of its plate like morphology and because of its presence and absence in various specimens. Within a week yet another paper was published on this new compound. The nature of the superconducting phase in yttrium palladium boride carbide was the product of work done in a German laboratory [12]. Here $YPd_5B_3C_{.3}$ was investigated by means of light-optical metallography, transmission electron microscopy and x-ray spectroscopy. This paper concluded that the superconducting phase was based on a structure and stoichiometry equivalent to that of $LuNi_2B_2C$ where Lu and Ni were replaced by Y and Pd respectivly, which was in agreement with the previous paper by Zandbergen. More recent work includes investigation of the boron partial isotope effect in Ni and Pd based systems conducted by a group at the University of Alberta [13]. Here it is reported that a shift in T_c occurrs of approximately 690 mK as natural Boron was replaced with the isotopes B^{10} and B^{11}. This shift supports electron-phonon mediated superconductivity, and in particular, the importance of phonons involving boron. This is in direct agreement with earlier work which proposed that superconductivity was based on the high frequency boron optical modes [14]. Based on previous research it seemed logical that high pressure work was the next step to take toward greater understanding of this system.

The objective of this research was to synthesize superconducting samples of $YPd_5B_3C_{.3}$, analyze the results of various magnetic and high pressure experiments and compare these

[2]High Resolution Electron Microscopy

results with those published. The data will then be used to determine several superconducting parameters. Chapter 2 of this thesis will encompass a brief review of relevant superconducting properties of both type I and type II superconductors. Those areas discussed include perfect conductivity and its difference from superconductivity as illustrated by the Meissner-Ochsenfeld effect and magnetic properties of both types of superconductors with special attention given to the difference between them. This will be followed by Chapter 3 where the reader is introduced to the experimental apparatus and the procedures used to obtain the data that will be discussed in the following chapter. The final Chapter will contain concluding remarks.

Chapter 2

Selected properties of superconductivity

2.1 Perfect conductors

In the superconducting state the dc electrical resistivity is zero or so close to zero that persistent electrical currents have been observed to flow without attenuation in superconducting rings for many years. The magnetic properties exhibited by superconductors are as dramatic as their electrical properties. The magnetic properties cannot be accounted for by the assumption that the superconducting state is characterized properly by zero electrical resistivity. Consider a perfectly conducting specimen that is cooled below its transition temperature T_c. Any closed circuit of such material has an important and useful property resulting from its zero resistance. The total magnetic flux threading a closed resistanceless circuit cannot change so long as the circuit remains resistanceless. This can only be so if the flux density at every point within the metal does not vary with time [15]. Consider the behavior of a perfect conductor under the following sequence of events. The specimen is cooled to some temperature $T_b \ll T_c$ and a magnetic field is applied. Since the flux density in the sample cannot change and the flux in the absence of the applied field was zero, it must remain zero even after the field is applied. If the magnetic field is then reduced to zero, the sample is again in its original unmagnetized condition (see Figure 2.1).

Now consider the same events but in a slightly different sequence. First the magnetic field is applied to the specimen at some temperature $T_a \gg T_c$ and then the specimen

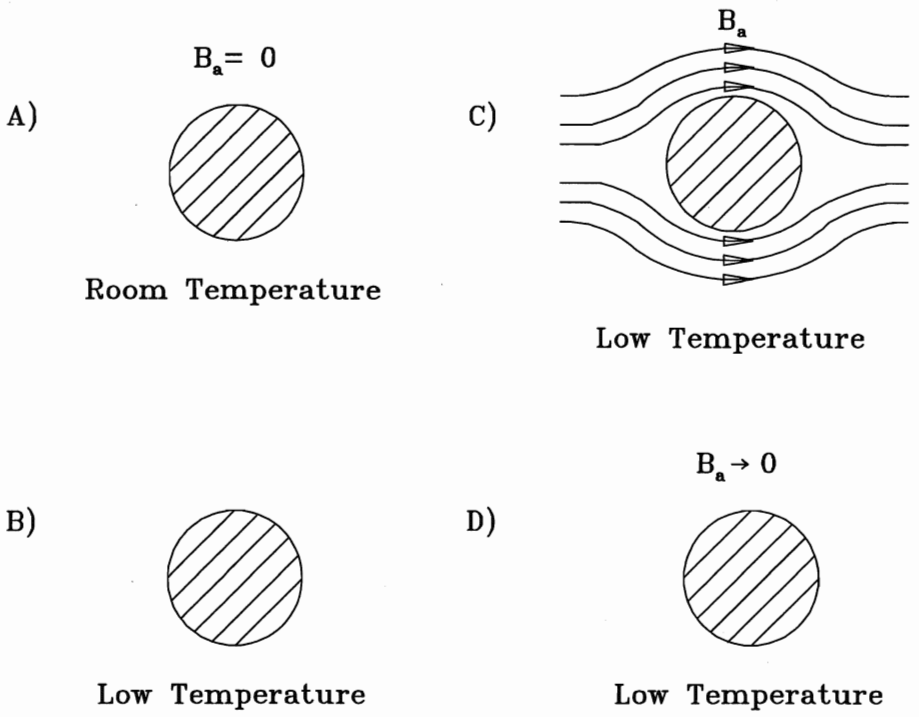

Figure 2.1: **Magnetic behaviour of a "perfect" conductor cooled in zero field**
a) and b) the specimen becomes resistanceless in absence of field,
c) Magnetic field is applied to the resistanceless specimen,
d) Magnetic field is removed (Adapted after [16]).

cooled below T_c. The loss of electrical resistance has no effect on the magnetization, and the flux distribution remains unchanged. The applied field is then turned off. As stated earlier the flux density cannot change as long as the closed circuit remains resistanceless and as a result the specimen is left permanently magnetized due to induced persistent currents that trap the flux inside the specimen (see Figure 2.2).

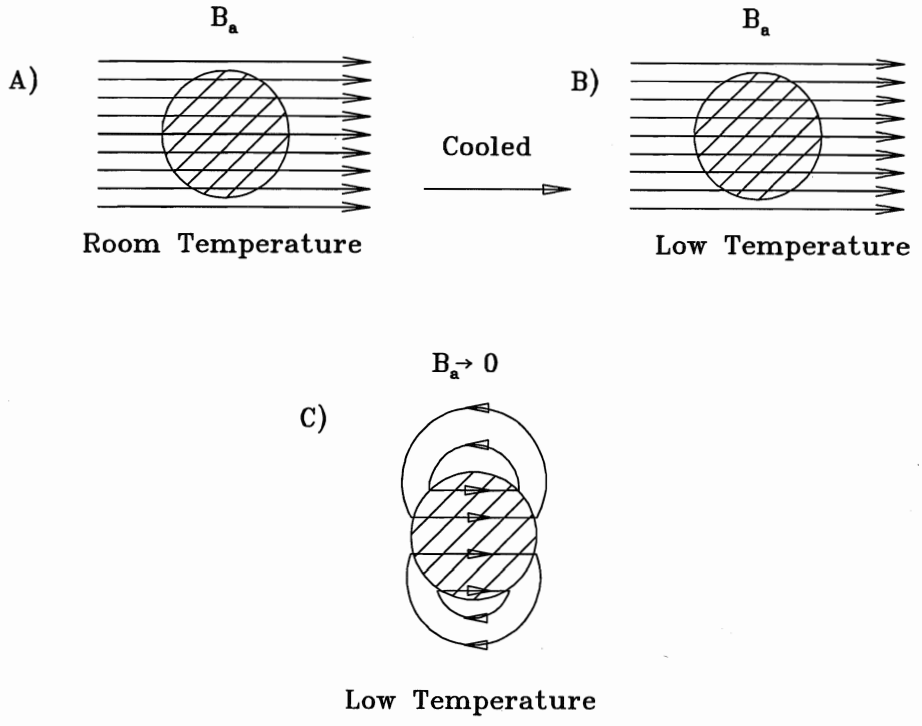

Figure 2.2: **Magnetic behaviour of a perfect conductor cooled in a field**
a) and b) the specimen becomes resistanceless in applied magnetic field.
c) Applied field is removed and the specimen is left permanently magnetized.

2.2 Meissner Effect

To illustrate the Meissner effect let us examine the result of utilizing the same progression as before, however this time our sample is superconducting. When a specimen is cooled below T_c and a magnetic field applied, the superconductor shields all magnetic flux from entering the interior of the sample. Removing the applied field leaves the sample unchanged from it's original unmagnetized state, and the result is no different than if the sample were a perfect conductor (Refer to Figure 2.1). Now when the superconductor is

cooled in an applied field, at T_c persistent currents arise on the surface. These currents are in fact induced by the application of the magnetic field and circulate on the surface of the specimen in such a manner as to create a magnetic flux density which is exactly equal and opposite to the flux density of the applied field. Since these currents do not die away, the net flux inside the specimen remains zero. This is illustrated in Figure 2.3 below. The surface currents **i** generate a flux density B_i that exactly cancels the flux density of the applied magnetic field B_a everywhere inside the metal. Removing the

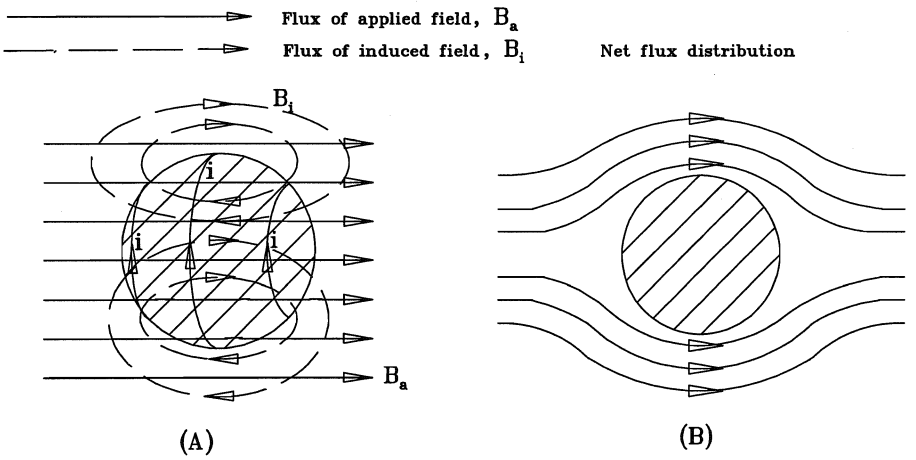

Figure 2.3: **Distribution of magnetic flux about a perfectly diamagnetic body**
A) Shows the flux distribution resulting from the combination of external flux and shielding currents,
B) The net flux distribution when $T < T_c$.

applied field results in the sample remaining unmagnetized, a result quite different than originally expected by Meissner and Ochsenfeld. This was the first experiment to show that superconductors are more than just perfect conductors. *Superconductors possess the unique property that never allows magnetic flux to exist in its interior regardless of the events leading to the application of the magnetic field.* A sample which exhibits no magnetic flux density is said to exhibit perfect diamagnetism.

2.3 Magnetization of Type II superconductors

This section is a discussion of the magnetic properties of type II superconductors. The development of the understanding of type II superconductors has involved strong interaction between theory and experimentation. As a group they are distinguished by a value of the Ginzburg-Landau parameter $\kappa > 1/\sqrt{2}$. The Ginzburg-Landau parameter is defined as

$$\kappa = \lambda/\xi \tag{2.1}$$

where λ is the magnetic penetration depth and ξ is known as the coherence length. The penetration depth is defined as the distance that an applied magnetic field may penetrate inside a superconductor until the field decays to $1/e$ of its value at the surface. The distance the flux may penetrate is given by:

$$\int_0^\infty B(x)dx = \lambda B(0) \tag{2.2}$$

where B(0) is the flux density outside of the sample and B(x) that within the sample. The sample is normal to a depth λ, the remainder is superconducting. In this range the number of superconducting electrons must rise dramatically from zero to a finite value. The distance that is required for this change is defined as the coherence length. Figure 2.4 is an illustration of the penetration depth.

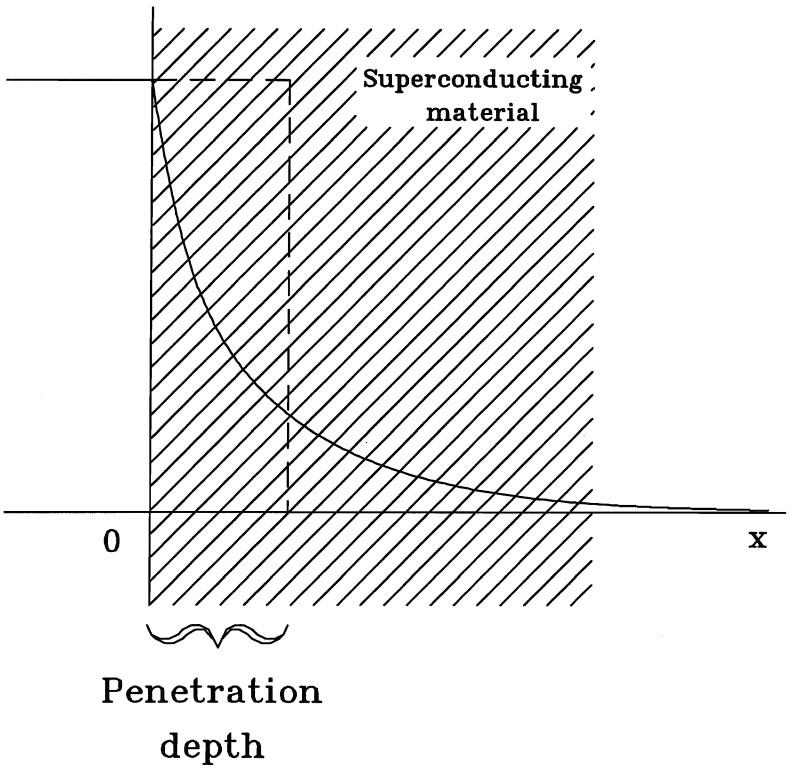

Figure 2.4: **Flux penetration into superconducting material,** The solid curve shows the exponential decay of the flux while dashed curve represents the definition of λ.

Consequently, macroscopic specimens of type II superconductors exhibit two superconductive phases in a magnetic field. These are a state of perfect diamagnetism as in type I superconductors and a state in which the magnetic induction, B, is finite. In this second phase the induction is associated with an array of supercurrent vortices in the specimen. Each vortex contains one quantum of flux, $\phi_0 = hc/2e \approx 2 \times 10^{-7} G \cdot cm^2$, so that a given B corresponds to B/ϕ_0 vortices per unit area [17].

A type II superconductor can be identified by the characteristic shape of the magnetization curve. The form of the ideal magnetization curve is given in Figure 2.5. Consider

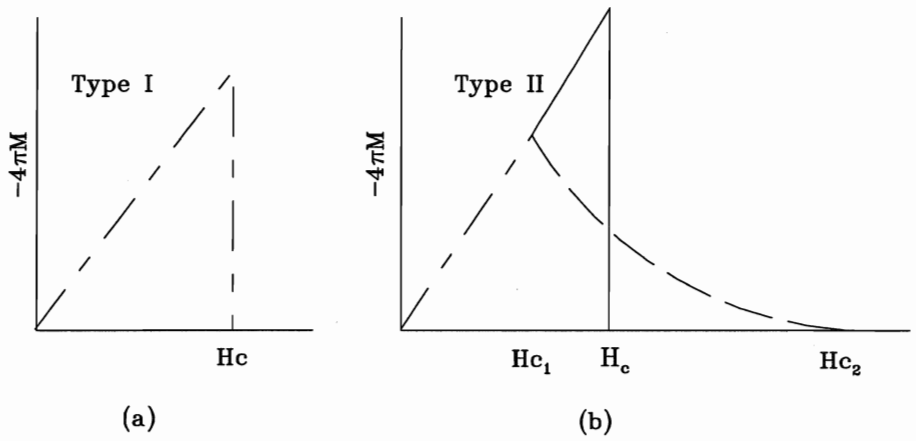

Figure 2.5: **Magnetization versus applied magnetic field**
a) for a bulk superconductor exhibiting perfect diamagnetism. A superconductor with this behavior is called a Type I superconductor. Above the critical field H_c the specimen is a normal conductor and the magnetization is too small to be seen. Note that minus 4πM is plotted on the vertical scale: the negative value of M corresponds to diamagnetism,
b) Superconducting magnetization of a Type II superconductor. The flux starts to penetrate the specimen at field H_{c1}. The specimen is in the vortex state between H_{c1} and H_{c2} where it has superconducting properties. Above H_{c2} the specimen is normal [18].

a type II superconductor in the shape of a long, cylindrical rod in a liquid bath maintained at some temperature T $< T_c$ and an external field is applied parallel to the axis of the rod. For fields less than the lower critical field, H_{c1}, the specimen exhibits perfect diamagnetism. The initial slope is unity, corresponding to a susceptibility χ of $-1/4\pi$ which follows directly from the Maxwell equation

$$4\pi M + H = B \tag{2.3}$$

where M is the magnetization, H the applied field and B the magnetic flux. For a perfect

diamagnet B=0, or

$$\frac{M}{H} = \chi = -\frac{1}{4\pi} \tag{2.4}$$

At $H_{c1}(T)$ the magnetization begins to increase until it vanishes at the upper critical field H_{c2} where the specimen becomes normal. The vortex state exists for $H_{c1} < H < H_{c2}$.

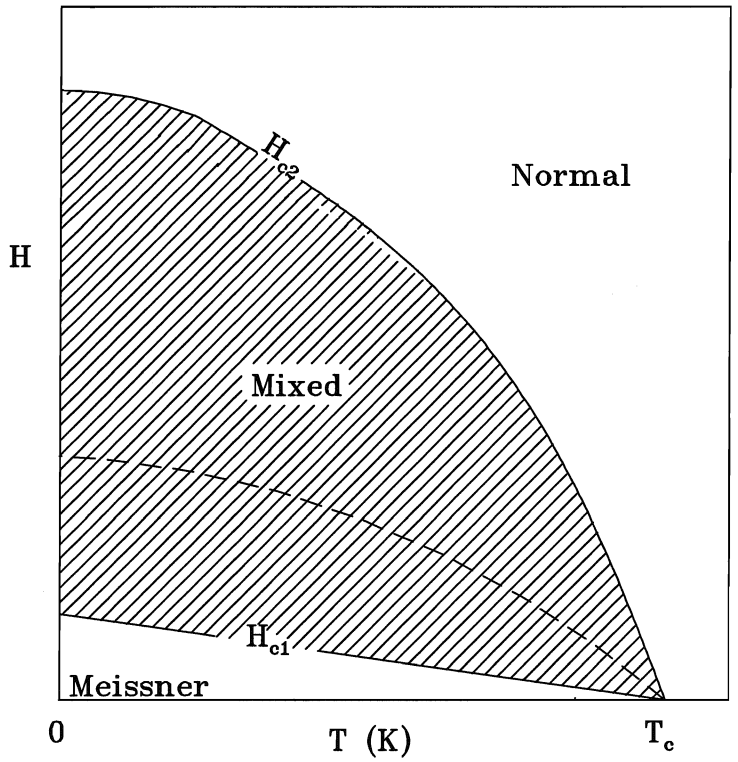

Figure 2.6: **Schematic diagram indicating how the critical fields divide the H-T plane**
Note the three distinct regions in which the phase is stable. At any point on a curve the two adjoining phases may exist in equilibrium. The dashed line denotes the thermodynamic critical field.

For long cylindrical samples of type I superconductors in a magnetic field parallel to the cylinder axis only two phases exist – the Meissner and normal phase. Consequently

the magnetization curve (Figure 2.5 a) is a right angle triangle. The area under the curve has magnitude $H_c^2/8\pi$. This represents the difference in Gibbs free energy between the normal and superconductive phases at a temperature $T < T_c$. For type II superconductors the area enclosed by the ideal magnetization curve equals the free energy difference between the state of perfect diamagnetism and the normal state. As a result it is possible to calculate the thermodynamic critical field by setting the area under the curve equal to $H_c^2/8\pi$. The thermodynamic critical field is shown in Figure 2.6 as a dashed line. It should be noted that $H_{c1} < H_c < H_{c2}$.

Figure 2.6 shows in general how the critical fields H_{c1} and H_{c2} depend on temperature. At a constant pressure, the curve divides the H-T plane into three regions. Points on a curve represent the values for H and T for which two phases may co-exist in equilibrium.

For magnetic fields $H_{c1} < H < H_{c2}$, tubes of flux-bearing (normal state) material occur in the superconductor. A tube of material is called a vortex and at its center the superconducting order parameter goes to zero. Along principal axes, the tubes are parallel to H, and current circulating around a vortex produces a magnetic field that screens the normal state vortex core from the superconducting region outside. *These surface currents are not transport currents*; rather, they are similar to the surface currents that shield the bulk of a type I superconductor (refer to Figure 2.3) yielding perfect diamagnetism [19]. Figure 2.7 shows such an arrangement of vorticies in an applied field. First impression may lead the reader to believe that this arrangement of superconducting and normal regions is distributed in a chaotic or non-ordered fashion. This would be incorrect. In fact they are arranged so as to reduce the overall free energy of the system. This is possible because of the *negative surface energy* created at the boundary between normal and superconducting regions which is larger than the increase in free energy due to the normal cores. The reader is referred to [15] for an explanation. It has been shown both experimentally [20] and theoretically that the most stable distribution of such fluxoids

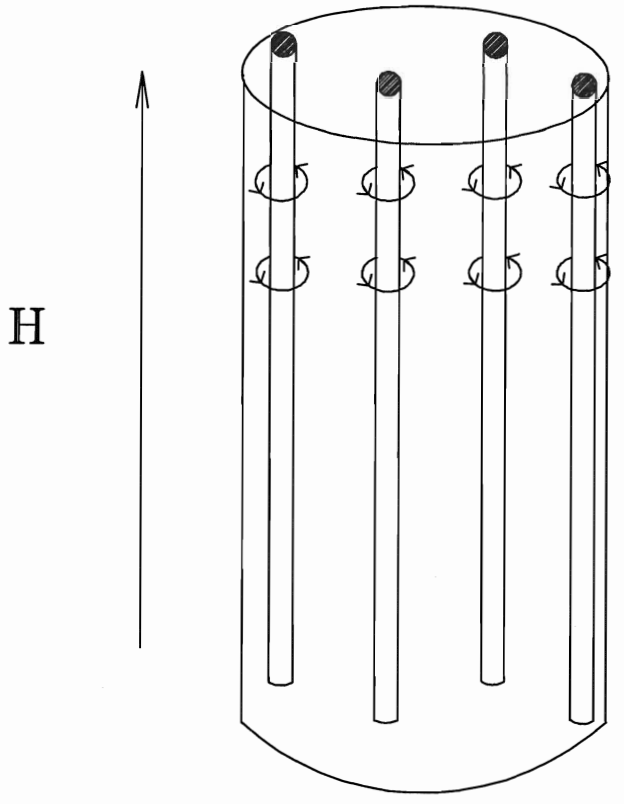

Figure 2.7: **Schematic diagram of pinned vorticies and the accompanying surface currents of a type II superconductor in an applied field H**

is a triangular array. Experimentalists must pay particular attention to the sequence of events leading to the transition from the vortex to normal state. Figure 2.8 illustrates that it is possible to acquire different results from the same sample if special attention is not given to the method used to obtain the data. If the magnetic moment of a sample was continuously measured as the magnetic field was slowly increased from zero to some value above the upper critical field and then reduced back to zero, different values of H_{c2} would be obtained. Their shape bear a striking resemblance to the ideal curve of Figure 2.5. The difference is due to flux trapping. As the field is increased the percentage of

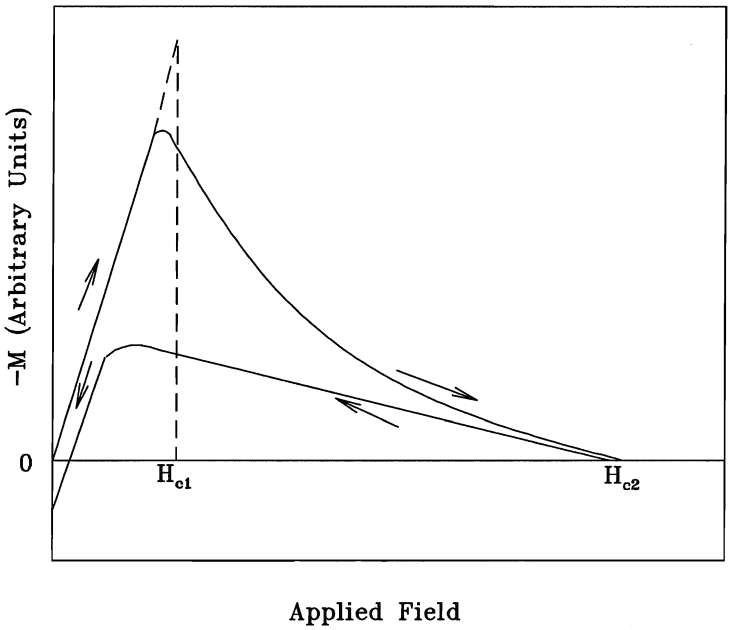

Figure 2.8: **Schematic drawing illustrating the irreversibility of magnetic moment measurement**
In increasing magnetic field there is a sharp break in the magnetization at H_{c1}, and a constant slope near H_{c2}. The curve however is not reversed when the field is reduced below H_{c2}.

normal cores continues to rise until the entire sample becomes normal at fields above H_{c2}. Now as the applied field is decreased and the sample reverts to the superconducting state, the magnetic moment of the sample is now different at a given field then it was just moments earlier when a field of the same magnitude was applied. This is due to flux pinning by the cores of normal material that were mentioned earlier and are shown in Figure 2.7. In effect the superconducting volume has been lowered because of the presence of the normal regions.

2.4 The critical temperature. Pressure effects

Pressure effects can provide some important clues for the understanding of the superconducting state. Particularly, the magnitude of variation of T_c under pressure, dT_c/dP, can test different theoretical models and may give some information regarding the origin of superconductivity in these alloys.

Three basic types of pressure techniques are in use today: (1) hydrostatic pressure transmitted by a fluid or gas which compresses the sample without deforming it plastically, (2) uniaxial stress obtained by subjecting the sample, normally a single crystal, to a uniaxial compressive or tensile force that is small enough not to exceed the elastic limit, and (3) quasihydrostatic pressure where the sample is surrounded by a solid pressure medium which transmits both hydrostatic and uniaxial stress to the sample, causing plastic deformation and introducing defects. Quasihydrostatic pressure techniques are widely used because the possibility of achieving pressures above 200 GPa [1]. However, the use of quasihydrostatic pressure in studies of superconductors should be approached with bridled enthusiasm. In Th_3P_4 structure compounds it has been shown that changing from hydrostatic to quasihydrostatic pressure will produce results of great difference, even to the extent that dT_c/dP changes sign [21]. The term "hydrostatic pressure" is used when the pressure medium remains fluid at the temperature when pressure is applied. Upon cooling, all fluids freeze below their melting temperature, but the shear stresses which then occur are far weaker than those generated during the course of quasihydrostatic pressure experimentation. Experiments under purely hydrostatic pressure conditions are well defined and yield results which can be compared to the predictions of theoretical models.

In studies of the superconducting state, the use of high pressure as a parameter has

[1] 1 GPa = 10kbar

the potential to make important contributions in several ways:

1. A rapid change of T_c with pressure is a distinct indication that the system under study is capable of achieving high values of T_c at ambient pressure if the system is suitably altered. In the $YBa_2Cu_4O_8$ system (Y124), which was found to exhibit a strong pressure dependence, substitution of Ca^{+2} for 10% of Y^{+3} causes an increase in the ambient pressure T_c from 75 K to 90 K [22].

2. Knowledge about the mechanism(s) responsible for superconductivity can be gained by searching for correlations between the pressure dependence of superconducting and normal parameters. For example in simple metal superconductors such as Pb or Al both T_c and $\rho(T)$ decrease under pressure because both are positive functions of the electron-phonon interaction, which decreases as the lattice stiffens [23].

3. The application of pressure can lead to structural changes, with the possibility of creating new phases with different or perhaps superior superconducting properties. Sintering under elevated oxygen pressure has been successful in the synthesis of Y124 [24].

4. Measurements of the hydrostatic and/or uniaxial pressure dependence of the superconducting properties can be used to check theoretical models [23].

It has been suggested that $YPd_5B_3C_{.3}$ is a conventional, electron-phonon coupled superconductor [25]. In reference [14] , it is proposed that superconductivity is based on high-frequency boron optical phonons, an idea further investigated by reference [13] and in agreement with [25]. In an attempt to explain the pressure dependence of the transition temperature of $YPd_5B_3C_{.3}$, it is useful, as a first approximation, to introduce the Bardeen-Cooper-Schriffer (BCS) [26] equation,

$$T_c \sim 1.14\langle\omega\rangle_{ph} exp[-1/N(E_f)V_{BCS}], \tag{2.5}$$

where $\langle\omega\rangle_{ph}$ is the average phonon frequency, $N(E_f)$ is the electronic density of states at the Fermi surface and V_{BCS} is a coupling constant. Within the BCS framework, pressure will influence T_c through variations of $N(E_f)$, changes in the phonon frequencies, or variations of the coupling constant V_{BCS}. The pressure dependence of $\langle\omega\rangle_{ph}$ will be dealt with first since it is the easiest to understand and its involvement remains unchanged regardless of the model chosen to describe the electronic density of states.

Recall the equation that describes the frequency of oscillation for a simple harmonic oscillator

$$\langle\omega\rangle_{ph} \propto \sqrt{\frac{k}{m}}. \tag{2.6}$$

Here m is the mass of the oscillating object and k is the spring constant. An analogy can be made between a harmonic oscillator and the atoms in a lattice. Imagine each atom as a small oscillator that is attached to each of its neighbours by a tiny spring of constant k. The application of external pressure to the lattice would cause the atoms to be forced closer together, increasing the depth of the potential well. As a result the value of the spring constant would become larger and therefore by equation 2.6 the frequency of oscillation $\langle\omega\rangle_{ph}$ would increase, leading to an increase in the transition temperature according to equation 2.5. However, there is a fundamental problem with the BCS equation; it fails to account for a decrease in the transition temperature of a system whose density of states at the Fermi level remains unaltered by the application of external pressure. In other words, any superconducting system whose electronic structure is dominated by flat s and p bands, in the eyes of the BCS equation, will experience an increase in T_c under pressure because only phonons will contribute to the change in the transition temperature.

Consider for a moment Figure 3.3 which illustrates the pressure dependence of the critical temperature of the simple metal Pb. Here $dT_c/dP \sim -10^{-3}$. Note also the

electronic structure of Lead: [Xe]$4f^{14}5d^{10}6s^2p^2$. Here the outer most electrons are the $6s^2$ and $6p^2$ orbitals, which are indicative of a flat density of states, hence only phonons would contribute to the pressure dependence of T_c. Consequently , BCS theory would predict that dT_c/dP of Figure 3.3 would be *positive, when in fact it is negative.* The problem with the BCS equation is that it is a simple approximation that fails to recognize the importance of phononic contributions, choosing instead to concentrate on the role of the electronic density in $T_c(P)$.

The McMillan equation [27]

$$T_c \sim \langle\omega\rangle_{ph} exp[-M\langle\omega\rangle_{ph}^2/N(E_f)V]\ldots \tag{2.7}$$

allows for a decrease in T_c under pressure when only phonons play a role. Here M is the ionic mass, V the matrix element of the electron-phonon interaction and $\langle\omega\rangle_{ph}^2$ is the square of the average phonon frequency. The heart of the equation lies in the exponential. The numerator is mainly phononic while the denominator is purely electronic. In the case of Lead, the denominator can be considered a constant because of the flat density of states. While under pressure the $\langle\omega\rangle_{ph}$ term will increase, causing an increase in T_c, however the $\langle\omega\rangle_{ph}^2$ will increase more rapidly. Since the exponential is negative and greater than the leading linear $\langle\omega\rangle_{ph}$ term, the net result is a loss of T_c under pressure, a fact previously unaccounted for using only the BCS equation.

Next, the involvement of the density of states will be addressed. The starting point will be the free electron model which will be followed by a discussion of an alternative approach known as the tight binding model.

2.4.1 Free electron approximation

Elements whose electrons move in an almost constant potential are often referred to as "free or nearly free electron" metals because the starting point for discussion is the

Sommerfield free electron gas, modified by the presence of a weak periodic potential. Consider for a moment the *free electron approximation* and equation 2.5. Here $N(E_f)$ $\propto K_f$ which in turn is proportional to $1/a$. K_f is the Fermi wave vector and a is the lattice parameter. This proportionality between K_f and a is a result of the solution of the density of states. For further details the reader is referred to references [18], [19] or [28]. The density of states is related to the energy , E, by the following

$$N(E) = \frac{\Omega}{4\pi^2}(2m/\hbar^2)^{3/2}E^{1/2}. \tag{2.8}$$

This relationship is shown in Figure 2.9. As pressure is applied to a solid the value of a will decrease, consequently both $1/a$ and K_f will increase in value. Since K_f is related to E_f by

$$E = \frac{\hbar^2 K^2}{2m} \tag{2.9}$$

it then follows that under pressure E_f will expand to a value E_f' and the density of states at the Fermi level will expand from value $N(E_f)$ to $N(E_f')$. This would result in a higher value of T_c.

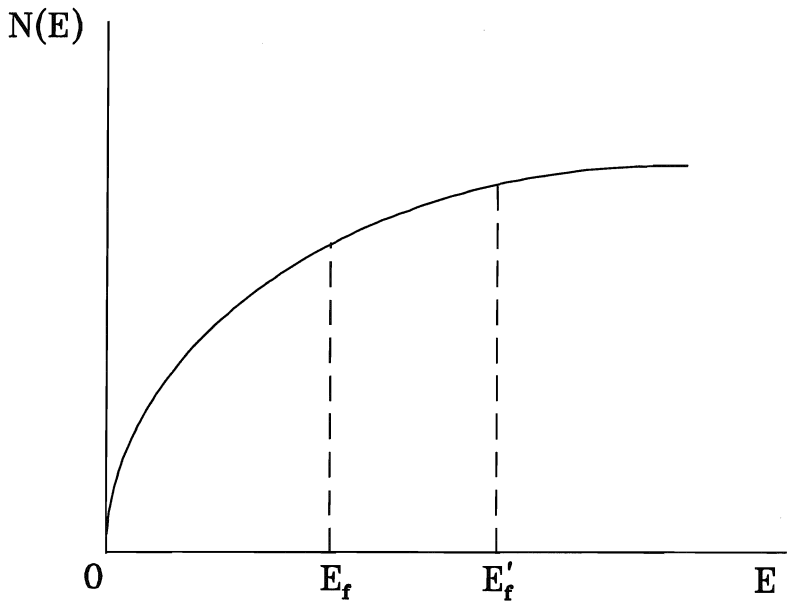

Figure 2.9: **The density of states for a free electron gas** Notice that for an increase in the level of the Fermi energy there is a corresponding increase in the density of states. As the level of the Fermi energy approaches its maximum value the change in the density of states in minimized.

2.4.2 Tight binding model

A significant difference between the *free electron gas approach* and the *tight binding model* occurs when calculating electronic levels. The *free electron approach* views the metal as a gas of nearly free electrons, only weakly perturbed by the periodic potential of the ions. We can take a much different approach, viewing the metal as a collection of weakly interacting neutral atoms. As an extreme example, imagine assembling a group of atoms on a cubic lattice with lattice constant of the order of one cm instead of an angstrom. All electrons would then be in atomic site levels localized at lattice sites, bearing little resemblance to the linear combination of plane waves found in the *free*

electron approximation.

If the imaginary lattice parameter of our metal were to shrink gradually, at some point before the true lattice parameter was reached the electronic levels would have to be modified. This would become necessary at some atomic level where the interatomic spacing approached the order of the spatial wave function because an electron would begin to feel the presence of its nearest neighbor, a fact unaccounted for in the *free electron approximation.*

The *tight binding model* deals with the case in which the the wave function overlap is large enough that corrections are necessary to the isolated atom approach. This approximation is most useful for describing the energy bands that arise from the d-bands of transition metals.

The three rows of the periodic table extending from the alkali earths (calcium, strontium and barium) to the noble metals copper, silver and gold contain the transition elements, in which the d-shell that is empty in the alkali earths is gradually filled. All are metals and their properties are dominated by the d-electrons.

Calculated transition metal band structures indicate that the d-band not only lies high in the conduction band but also extends into the Fermi level. When levels on the Fermi surface are d-derived, the tight-binding approximation is a better starting point for estimating the Fermi surface than the *free electron approximation* [28].

The d-bands typically are narrower than free electron conduction bands and are capable of containing 10 electrons. As a result of being narrower and being able to house more electrons in a narrower energy range than both s and p bands, the density of states is likely to be much higher [29]. This effect can be observed in the electronic contribution to the low temperature specific heat.

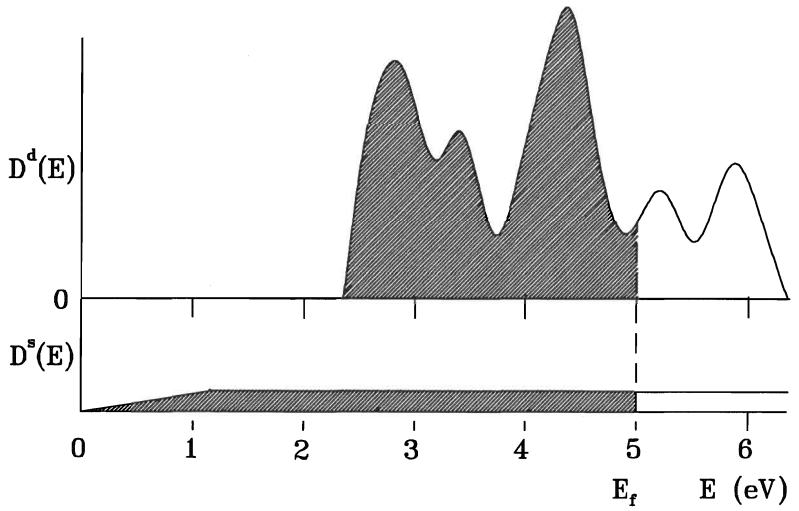

Figure 2.10: **Qualitative features of the d-band and s-band contributions to the density of states of a transition metal**
The d-band is narrower and contains more levels than the s-band, consequently when the Fermi level (separating the shaded and unshaded regions) lies within the d-band the density of states is much larger than the free-electron like contribution of the s-band alone.

Focusing on the influence of pressure on $N(E_f)$, the application of pressure can be viewed as increasing the density of carriers per unit volume, thereby shifting E_f to higher energies. A better understanding of $T_c(P)$ could be obtained if the exact shape of the density of states around the Fermi level and the initial position of the Fermi level at zero pressure were known. None the less , a qualitative approach is possible. Within the tight binding model, it would be possible to explain either a positive or negative change in T_c under pressure. For instance, if dT_c/dP is positive, this could be attributed to the applied pressure moving the Fermi level from the low side of a peak in the density of states to the high-side. Conversely, if the dT_c/dP is negative, it is possible that pressure has moved the Fermi level from the high-side of a peak to the low side. This method also has the advantage of being able to explain very large changes in T_c because of the

complex structure of the density of states of a transition metal (see Figure 2.10 whereas the *free electron approximation* allows only very flat band structure and is unable to account for large changes in T_c, either positive or negative.

Chapter 3

Experimental Details

3.1 Sample Preparation

3.1.1 Arc-Melting

Samples were prepared by an arc-melting technique. Starting materials were Y foil (99.99% purity), Pd wire(99.99% purity), and coarse powders or single crystals of C (99.99% purity) and B (99.99% purity). Appropriate amounts of the high purity element metals were weighed using a Fisher scientific balance to obtain the desired composition; the total weight was usually about 1 gram. For optimum operating conditions, the vacuum chamber was evacuated using both mechanical and diffusion pumps and flushed twice with argon gas in an attempt to remove oxygen from the system. In an effort to be certain of the presence of little or no oxygen in the vacuum chamber a zirconium getter was melted to absorb oxygen not removed by the pumps. The metals were then arc-melted for 10 seconds on a standard water cooled copper hearth under high purity argon gas using a tungsten electrode. To ensure homogeneity the resultant pellets were then turned over and arc-melted a second time. Initially all constituents were arc-melted together, however this method was inadequate as it did not allow one to observe the percent loss of each individual element. It was necessary to ensure that each metal was present in the compound as all four elements were required for superconductivity to exist. Our problem was ensuring that the proper amount of Boron was present in the sample. Due to its low mass and the sudden application of a very large current, Boron was very

likely to 'fly away'. To avoid such a loss it was decided that Boron should be added to a known mass of one of the constituent metals, arc-melted and reweighed. The difference in mass before and after arc-melting was due to the addition of Boron. This process was repeated until the desired ratio was achieved.

3.2 Resistivity

To a small piece of flat, sanded sample, four gold wires were spot welded. Great care was taken to ensure good contacts. The sample was then fastened to a holder and a standard, computer-automated, four point dc resistivity technique was used to measure the transition temperature of the superconducting sample. A constant current of 5 mA was passed through the two outer wires as the voltage was measured across the sample. To overcome possible error due to the presence of thermal emf, the direction of the d.c. current was reversed and the average of the two voltage readings was taken. Temperature was monitored by a calibrated thermometer and the computer interface allowed data to be taken at regular intervals.

3.3 Magnetic Measurements

All magnetization measurements were performed using a Quantum Design dc SQUID magnetometer. The normal measurement technique used was to position the sample below the detection coils and then raise the sample through the coils while measuring the output of the SQUID magnetometer. In its initial position, the sample should be far enough below the detection coils so that the SQUID does not detect the sample moment. The sample is then typically measured by repeatedly moving the sample upward some distance and reading the voltage from the detector. It is then possible to plot voltage as a function of sample position. This procedure allows a quick scan of the sample so that it

is possible to verify that the sample is positioned properly between the pick-up coils [30]. The shape of the curve is a function of the detection coil geometry used in the MPMS[1]. The coils are wound in a second derivative configuration in which the upper and lower single turns are counterwound with respect to the two turn center coil (see Figure 3.1). This configuration strongly rejects interference from nearby magnetic sources and allows the system to function without a superconducting shield around the SQUID sensing loop.

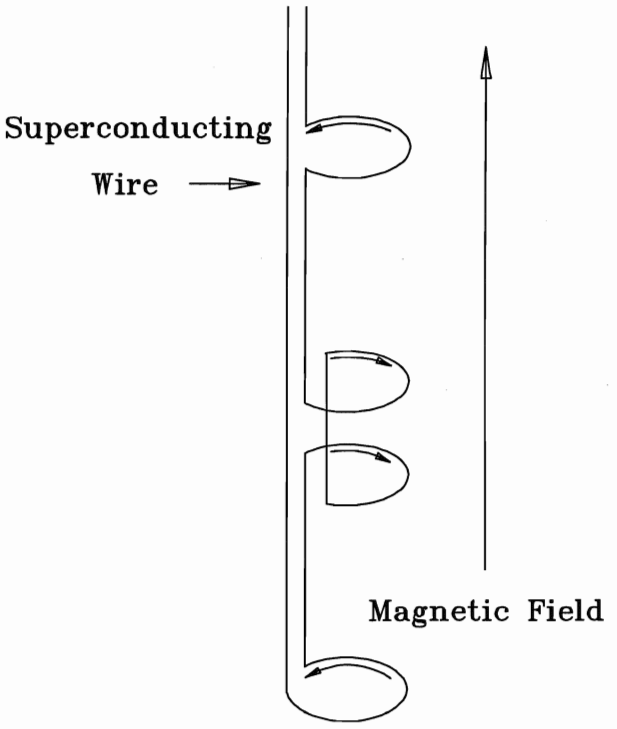

Figure 3.1: **Second Derivative Coil Configuration**

A valuable technique is to mount the sample on a long uniform rod which serves as the sample holder. If the sample is in the middle of the rod so that the holder extends completely through the coils, the resulting signal in the SQUID detector will represent

[1]Magnetic Property Measurement System

the sample only. In this case the holder represents a uniform background to the closely spaced second derivative coils; only the signal from the sample remains. With this in mind the sample was spring loaded into the center of a plastic drinking straw which was then in turn attached to the commercial measuring rod with a small wire. This unit was then inserted into the magnetometer.

Magnetoresistance measurements were carried out on polycrystalline $YPd_5B_3C_{.3}$. Four gold wire contacts were spot welded to the sample surface, to which four leads were then indium soldered. To carry out the measurements the sample was placed inside the SQUID magnetometer where the temperature and applied field were controlled. Since the magnetometer was not designed for this type of measurement data was recorded manually. Initially the sample was cooled to the desired temperature in zero field to avoid any flux trapping. Once the set temperature was reached a magnetic field was applied. A constant d-c current was then passed through the sample and the corresponding voltage was recorded. To avoid any thermo induced voltage the polarity of the current was reversed and an average of the measured values was recorded. At each temperature interval the field was swept up from zero until the sample was driven normal. The temperature was then raised above T_c, the applied field set to zero and the sample was again zero field cooled.

3.4 Hydrostatic Pressure Measurements

The superconducting transition temperature of $YPd_5B_3C_{.3}$ was measured as a function of increasing pressure up to $\approx 13kbar$ using an appropriate hydrostatic pressure cell. The high pressure apparatus consists of a Cu-Be pressure cell and a lead manometer. The sample was first sanded to a thickness of 90 microns and placed in an ultrasonic bath using both acetone and propanol to ensure surface cleanliness. The sample, fastened

using GE varnish, and a small ribbon of lead (used to monitor pressure in the cell) were then attached to a piston shaped holder. Four gold wire contacts were then spot welded to the surface of the sample under an argon atmosphere to avoid oxidation of the sample surface. These gold leads were then soldered to existing wires as was the lead ribbon. This holder was then fitted into a kerosene filled cell. The entire apparatus was able to measure the superconducting transition temperature of both the metallic and lead samples simultaneously using a four-point dc resistivity technique. The apparatus used in this particular experiment is shown schematically in figure 3.2.

Pressure was applied to the cell by two opposing tungsten carbide pistons. The cell is pressure loaded using a commercial hydraulic press and the pressure is then frozen in by a locking screw. First the area between the outer dewar and cryostat wall was evacuated to provide insulation from room temperature surroundings. The apparatus is then cooled in a standard cryostat in stages. First, the outer dewar is filled with liquid nitrogen and the sample is cooled to $\approx 170K$. Next liquid nitrogen is transferred directly into the inner dewar until a temperature no less than 120 K is reached. Finally liquid helium is transferred until the sample reaches a temperature in the vicinity of 4 Kelvin. It is very important that the temperature during the second stage of cooling not approach the temperature of liquid nitrogen otherwise liquid nitrogen may begin to accumulate in the inner dewar. This nitrogen will freeze when liquid helium is transferred to the system, making it impossible to cool below 77 K. If liquid nitrogen did accumulate it was immediately pumped out. Once the cell was stabilized at liquid helium temperature, data acquisition began. The pressure cell was manually lifted slightly above the level of liquid helium in the inner dewar and allowed to warm very slowly. Sample and lead voltages were measured every .05 K when the temperature was within 3 K of their respective transitions. After the transition temperature of the metallic sample was reached the entire cell was then lowered into the liquid helium , the temperature was allowed to

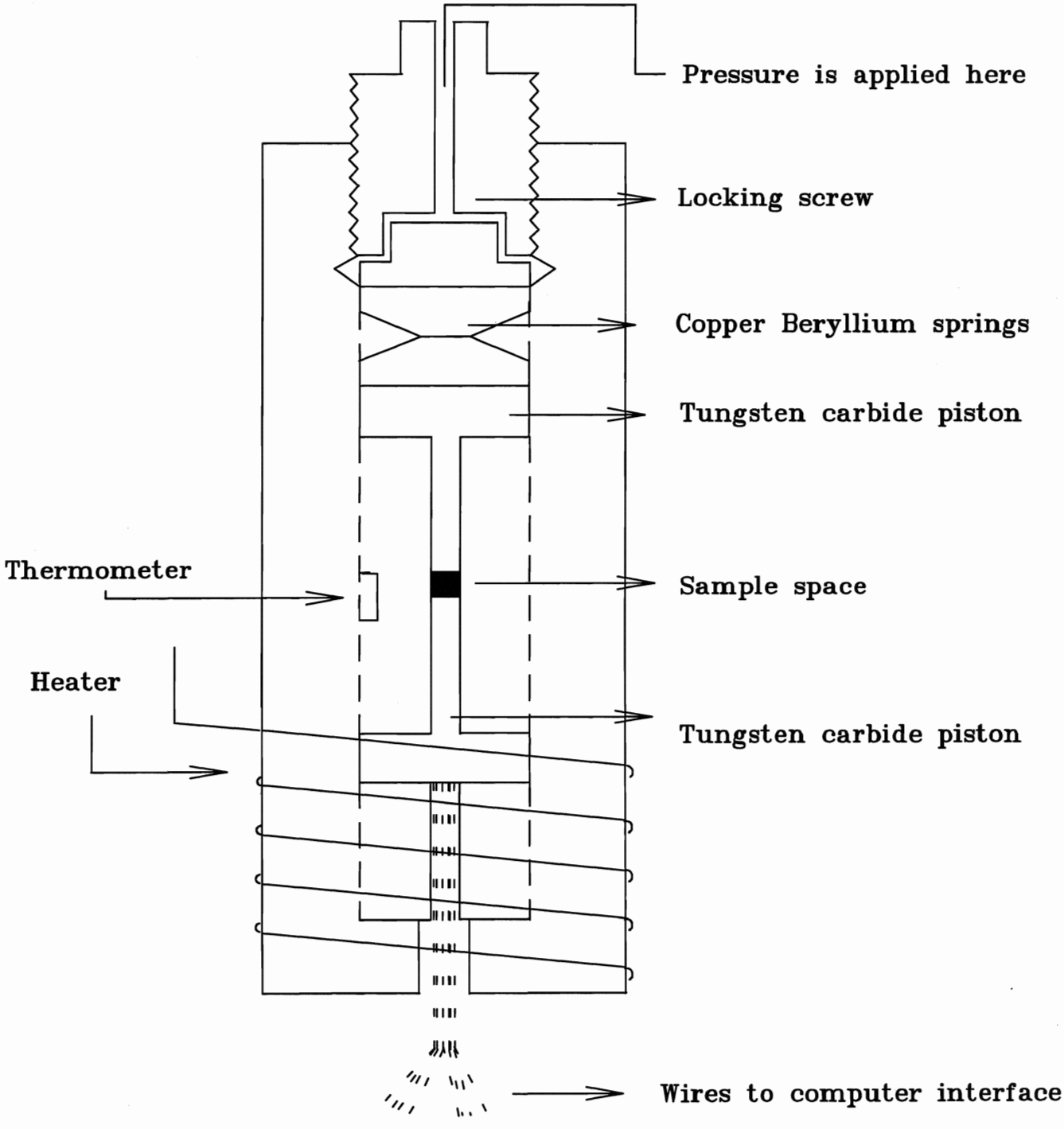

Figure 3.2: **Schematic drawing of Hydrostatic Pressure Cell** (Adapted after [31]).

stabilize and the procedure was repeated.

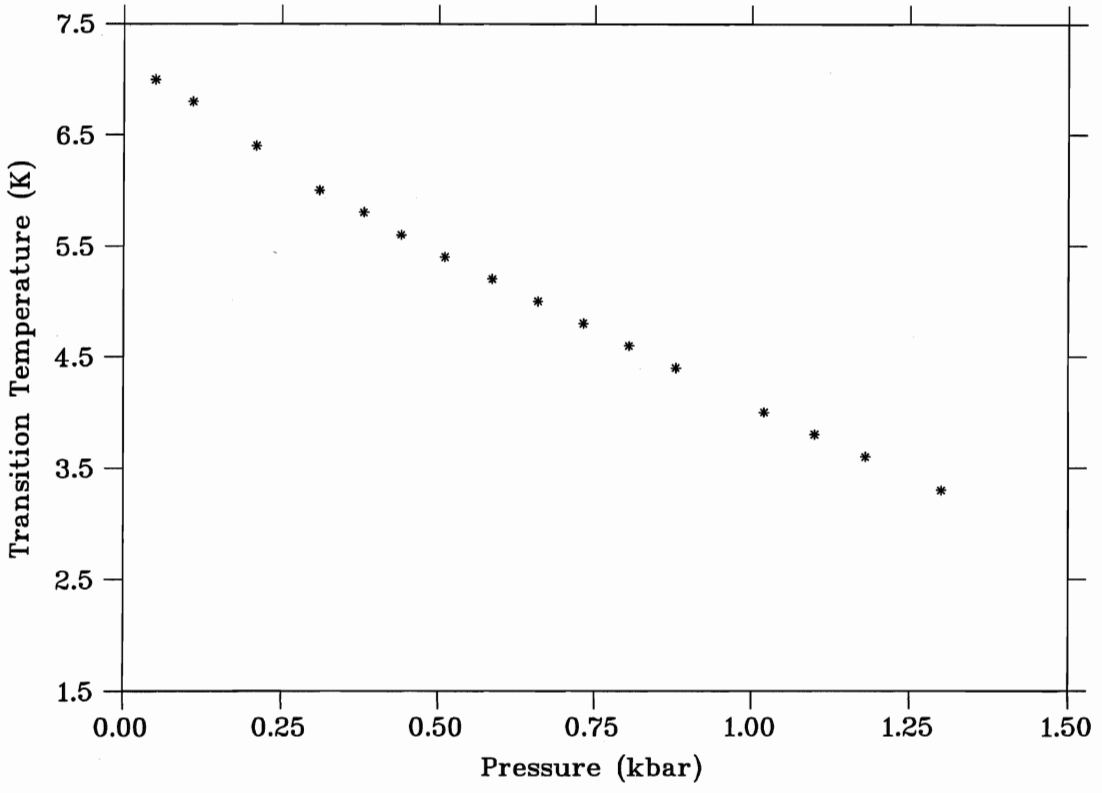

Figure 3.3: **Superconducting Transition Temperature of Lead vs Pressure**
(After [32]).

Accurate temperature readings were crucial in determining the success or failure of any trial run, since use of a lead manometer is based on the Eichler and Witting [32] curve which relates the T_c of lead to the applied pressure (Figure 3.3). A good thermometer is one which permits sufficient sensitivity with the smallest heat dissipation in the thermometer itself. It is also desirable that the voltage or some simple function of it vary linearly with temperature since this facilitates the conversion of voltage to temperature. Temperature in the cell was monitored via a calibrated Silicon diode thermometer (Figure 3.4) located very close to the sample to minimize any possible temperature gradient.

As is evident from Figure 3.4, the thermometer used in this experiment met the desired criteria in the temperature range below 25 K, the range of interest in this experiment.

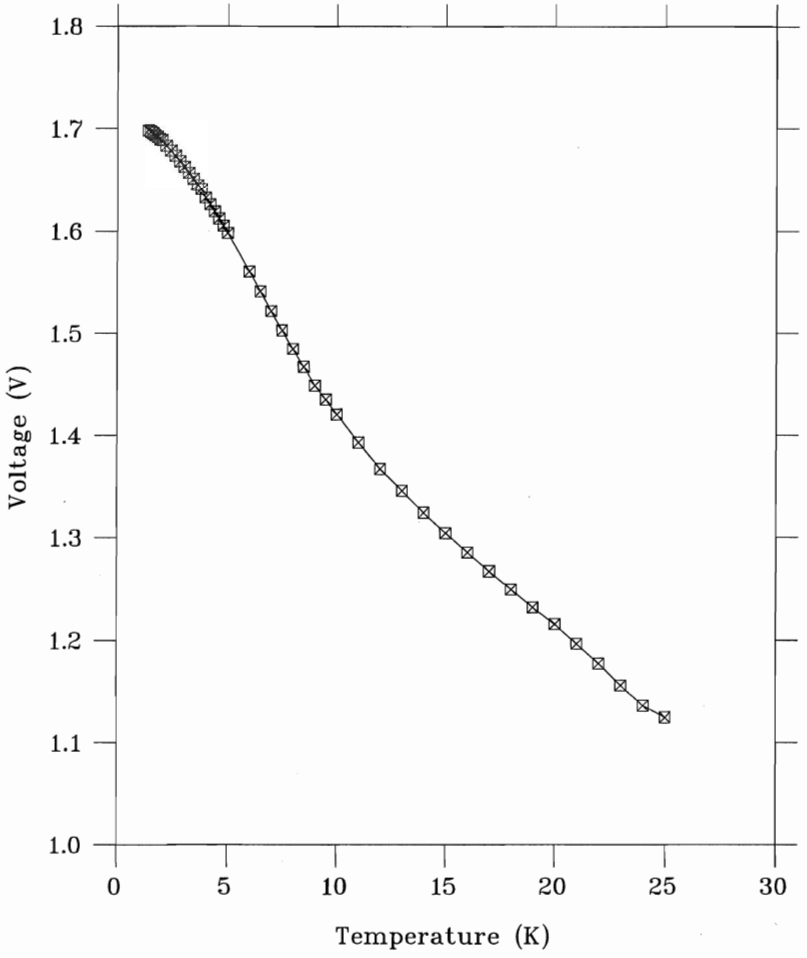

Figure 3.4: **Thermometer Calibration.** After [33].
Note the near linear relation between voltage and temperature, a desirable criteria for temperature conversion.

Chapter 4

Experimental Results and Discussion

4.1 $YPd_5B_3C_{.3}$

Reports of superconductivity in $LuNi_2B_2C$ [34] preceded those of $YPd_5B_3C_{.3}$. The $LuNi_2B_2C$ has a fairly simple structure, which is based on the stacking of LuC layers with Ni_2B_2 blocks in between . In contrast with the Lu-Ni-B-C system, in which the superconducting phase was easily identified, it was reportedly difficult to determine the superconducting phase in the system Y-Pd-B-C . The superconducting specimen $YPd_5B_3C_{.3}$ contains six phases, one of which is the proposed superconducting phase YPd_2BC (see Figure 4.1) [8]. The 23 K superconducting phase is tetragonal body-centered with lattice parameters a=3.78 Å and c=10.81 Å. It is possible that one of the other phases is superconducting, however this is unlikely since only YPd_2BC consists of extended plates which can easily form an interconnecting network allowing zero resistance and the large magnetic screening below T_c [11] to occur, whereas all other phases form isolated crystals which are unlikely to allow a path of zero resistance unless they are abundant. It then follows that the sample used in this study most certainly has at least two of the six phases mentioned by previous authors, one of which must be the superconducting phases YPd_2BC. X-ray diffraction measurements on the system were found to agree well with those reported elsewhere [35]. It should be noted that it is possible that the sample contains other phases however it was not possible to identify them or be certain of their existence.

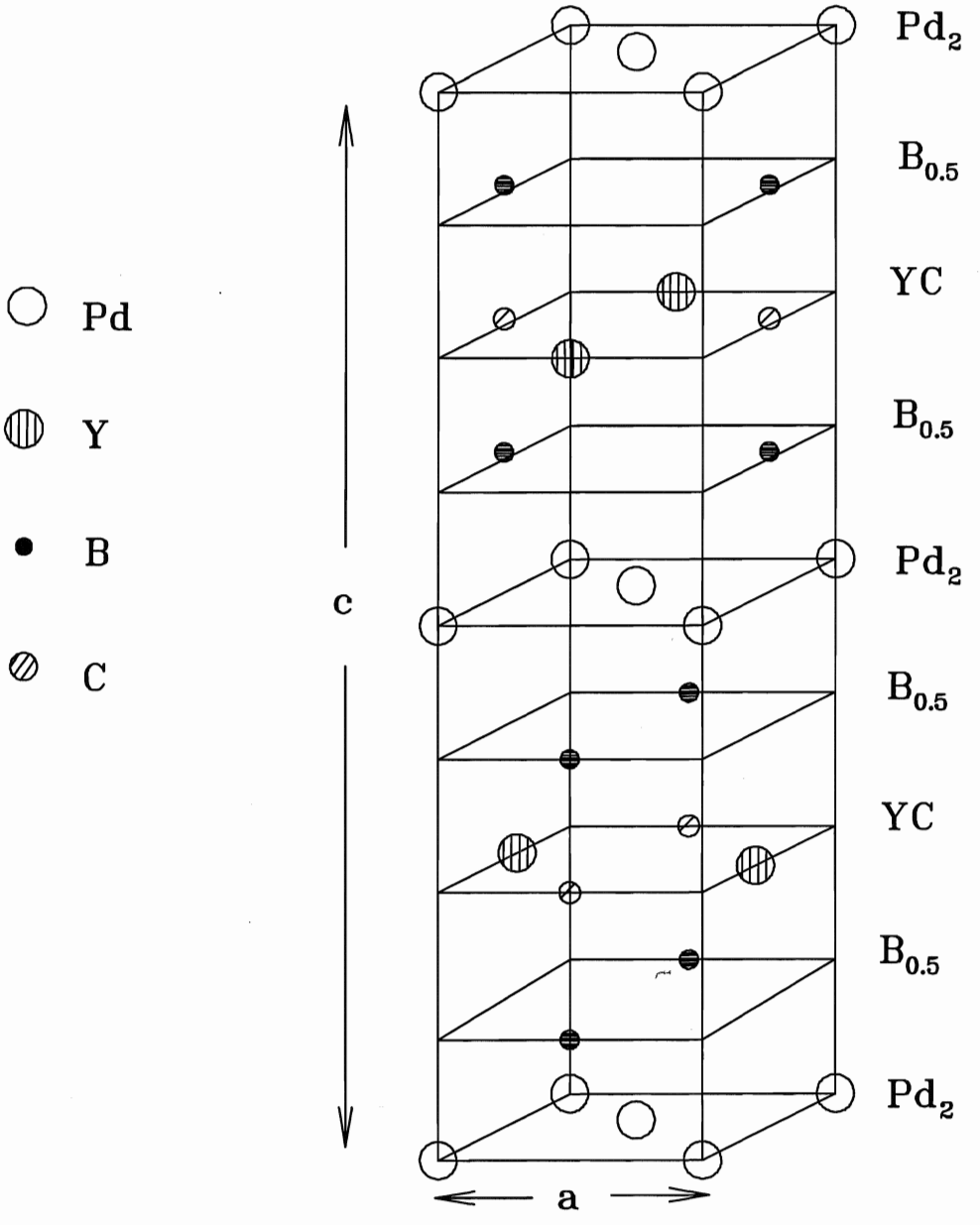

Figure 4.1: **Schematic representation of the proposed superconducting structure** YPd_2BC
The 23 K superconducting phase is tetragonal body-centered with lattice parameters a =3.78 Å and c=10.81 Å.

4.2 Resistivity

Figure 4.2 shows the temperature dependence of the resistivity for a polycrystalline sample of composition $YPd_5B_3C_{.3}$. The normal state resistivity is of the order $.15\mu\Omega cm$ at

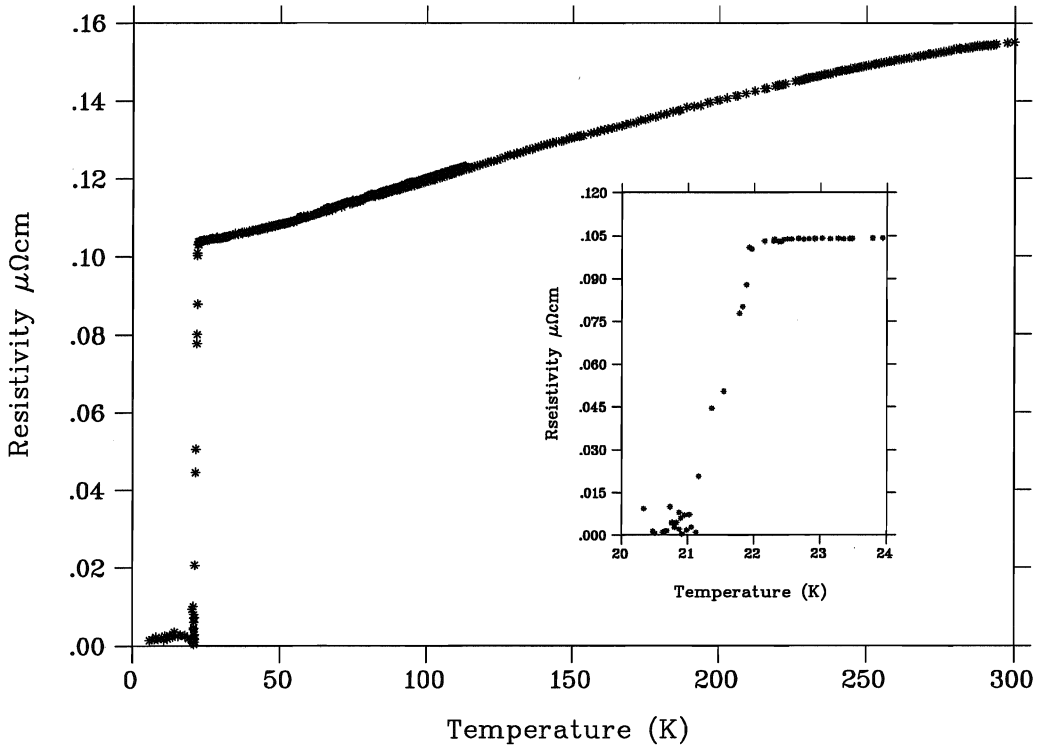

Figure 4.2: **Temperature dependent resistivity of** $YPd_5B_3C_{.3}$
Inset shows expanded view of the superconducting transition.

room temperature, and shows a slight "S" shaped temperature dependence. The resistivity exhibits normal metallic behavior, namely, it decreases with decreasing temperature. The inset to Figure 4.2 shows the resistive superconducting transition in more detail. The 10-90% transition width is $\sim 1K$, and the onset temperature is 22.0 K.

4.3 Magnetization

4.3.1 Field dependence of the magnetization

Lower critical field

In principle H_{c1} and H_{c2} can be obtained directly from the M versus H curve. H_{c1} is determined as the field at which M deviates from linearity and H_{c2} is the field at which the magnetization M goes to zero. An example of a typical field dependent magnetization curve for $YPd_5B_3C_{.3}$ in the superconducting state is shown in Figure 4.3 at 5 K. Field

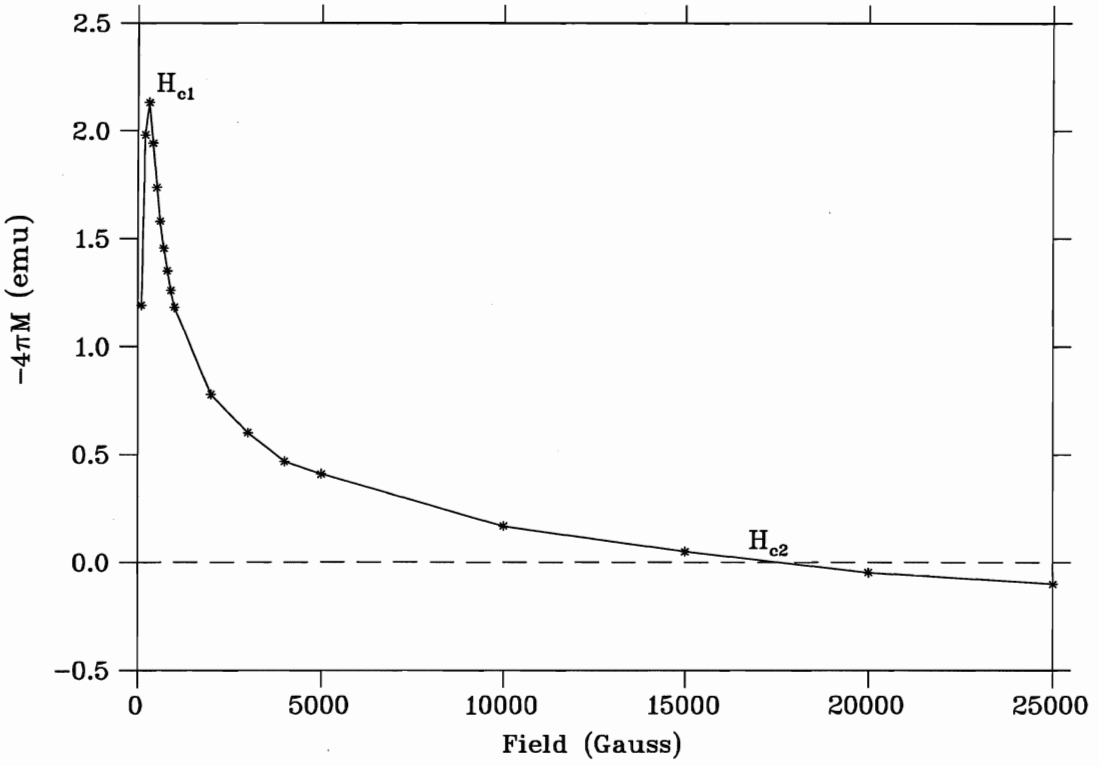

Figure 4.3: **Field dependence of the magnetization of $YPd_5B_3C_{.3}$ at constant temperature 5 K.**
The lines drawn are a guide for the eye.

dependence of the magnetization has been investigated for the temperature interval 2 to

21 K . Values of the lower critical field were calculated by fitting the low field data linearly using least squares analysis and noting the field where the experimental curve deviated from the fit. Figure 4.4 shows the low field data obtained at 5 K. The measurements were performed on a long bar-shaped sample that was cut from the melted pellet to a length not exceeding 3 mm. The sample was then measured, its orientation unaltered for subsequent measurements.

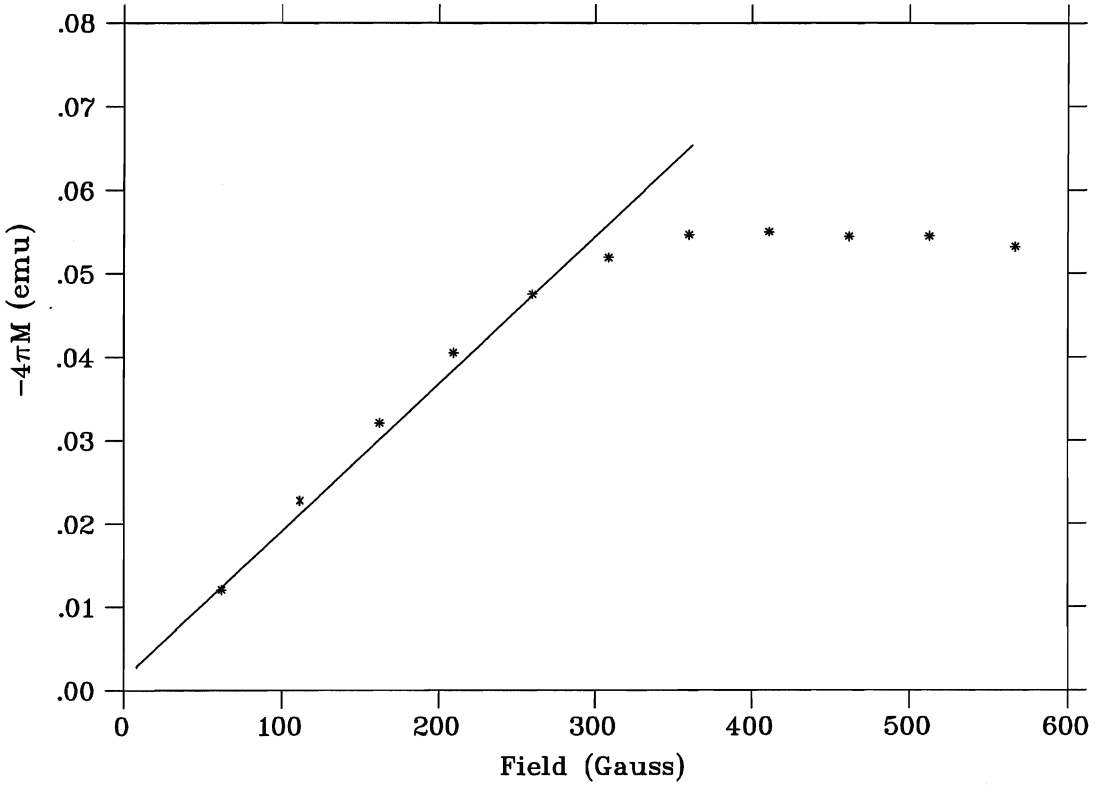

Figure 4.4: **Low field magnetization versus field for** $YPd_5B_3C_{.3}$
The solid line represents a least squares fit to the low field data.

The result of fitting the low field data is given in Figure 4.5. The plot is very close to an ideal curve. The slope of the field at low temperatures is nearly zero and the value of the lower critical field falls rapidly as T_c is approached. Because the superconducting

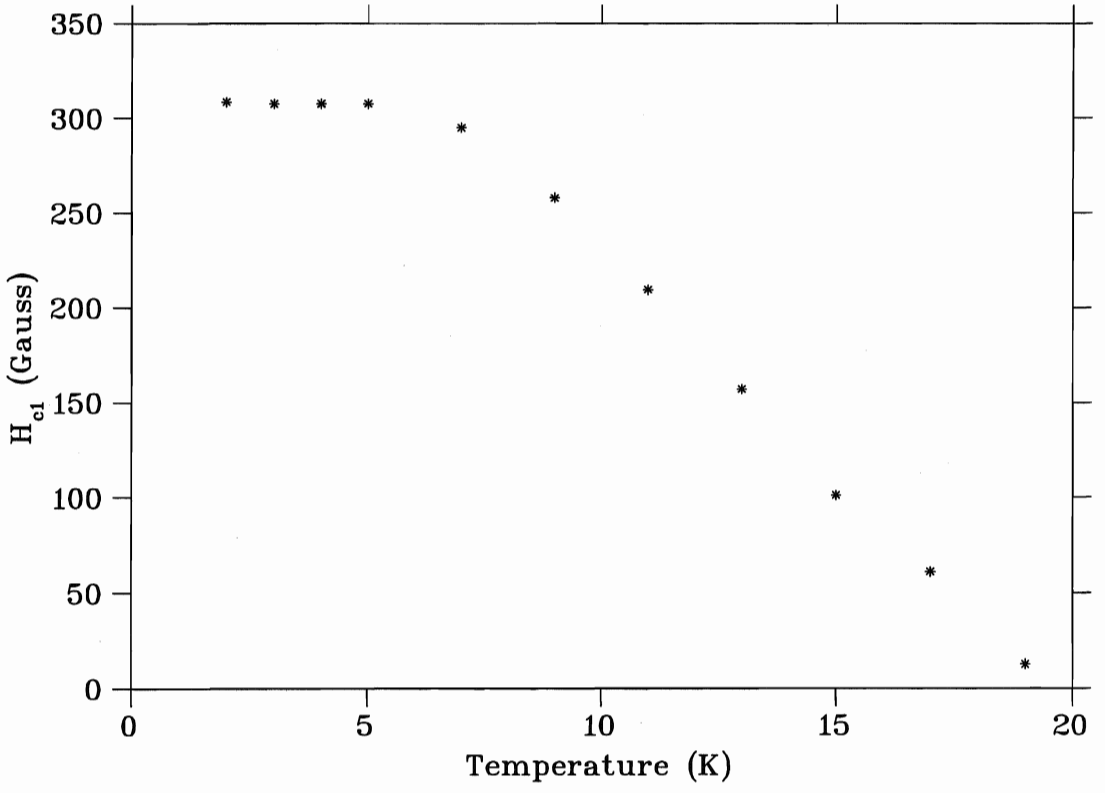

Figure 4.5: **The lower critical field as derived from linear least squares fit.**

phase has not been isolated for the Y-Pd-B-C system, it is premature to perform detailed characterization at this stage. In the mixed phase $YPd_5B_3C_{.3}$ sample, the lower critical field is roughly estimated from Figure 4.5 to be 310 Gauss at 5 K.

Upper Critical Field

In Figure 4.6 we show magnetization as a function of field. In the case of a perfect diamagnet it would follow that the upper critical field occurs where the magnetization becomes zero. However, this approach yields $H_{c2} \sim 55000$ Gauss at low temperatures, a value comparitively smaller than those previously published [10]. As illustrated in figure 4.6 the *magnetization* not only goes to zero but in fact continues in the positive direction. It is believed this discrepancy is due to electronic paramagnetism, which can be much reduced in the superconductive and vortex phases, so that in a field the normal free energy is reduced relative to the vortex phase by this effect. This has the consequence of reducing H_{c2}. In an attempt to remove this paramagnetic response and find the true

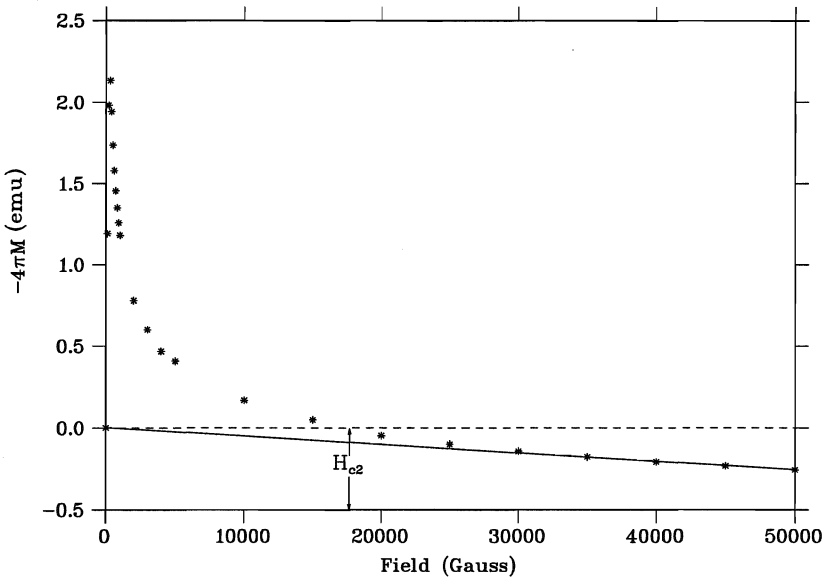

Figure 4.6: **High field dependence of the magnetization of $YPd_5B_3C_{.3}$ at 15 K.**
The raw data obtained directly from experiment is shown. The solid line represents the least squares fit used to remove the paramagnetic response from the raw data at high fields. The dashed line at M=0 is to aid the reader in locating H_{c2}.

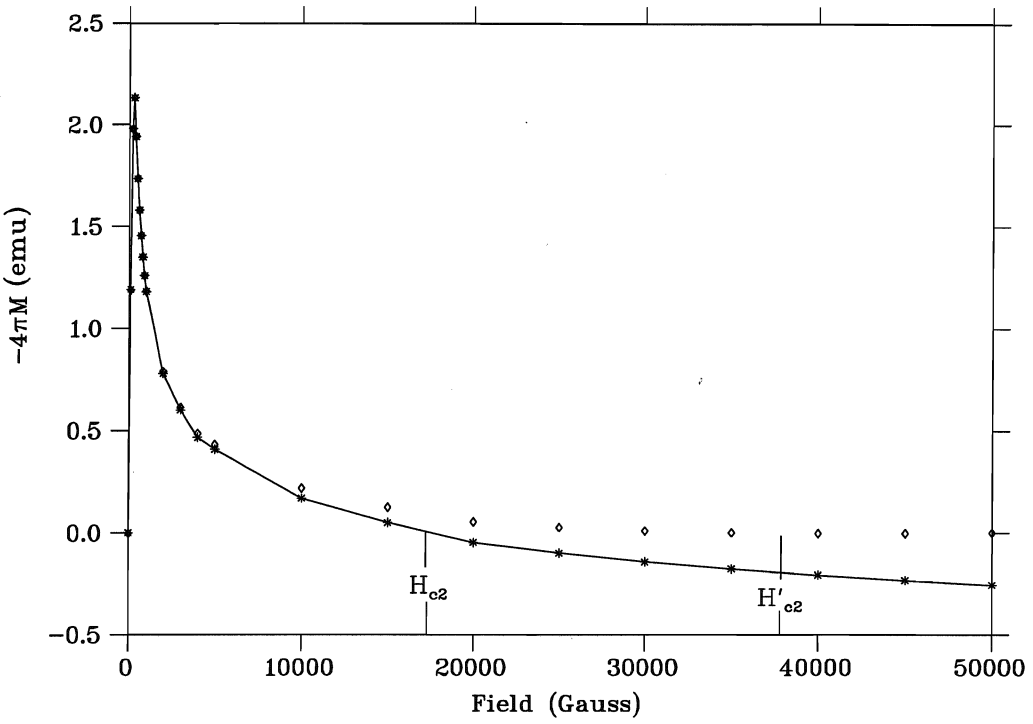

Figure 4.7: **An overlay of the raw and corrected data for the field dependence of the magnetization of** $YPd_5B_3C_{.3}$
$\star$ represents the original raw data,
$\diamond$ denotes the data which has been fitted and the paramagnetic response subtracted.

value of H_{c2} least squares analysis was performed on the high field data. A line of best fit was calculated for the high field data and this correction was then subtracted from the raw data. The true value of H_{c2} was then taken as the field where the magnetization approaches zero. Figure 4.7 is presented to the reader to illustrate the difference in H_{c2} values obtained using the two methods. The original, raw data is represented by $\star$ while $\diamond$ denotes the data which has been fitted and the paramagnetic response subtracted. Figure 4.8 shows the temperature dependence of the upper critical field obtained using the two methods. T_c extrapolted from resistance measurements is 23 K.

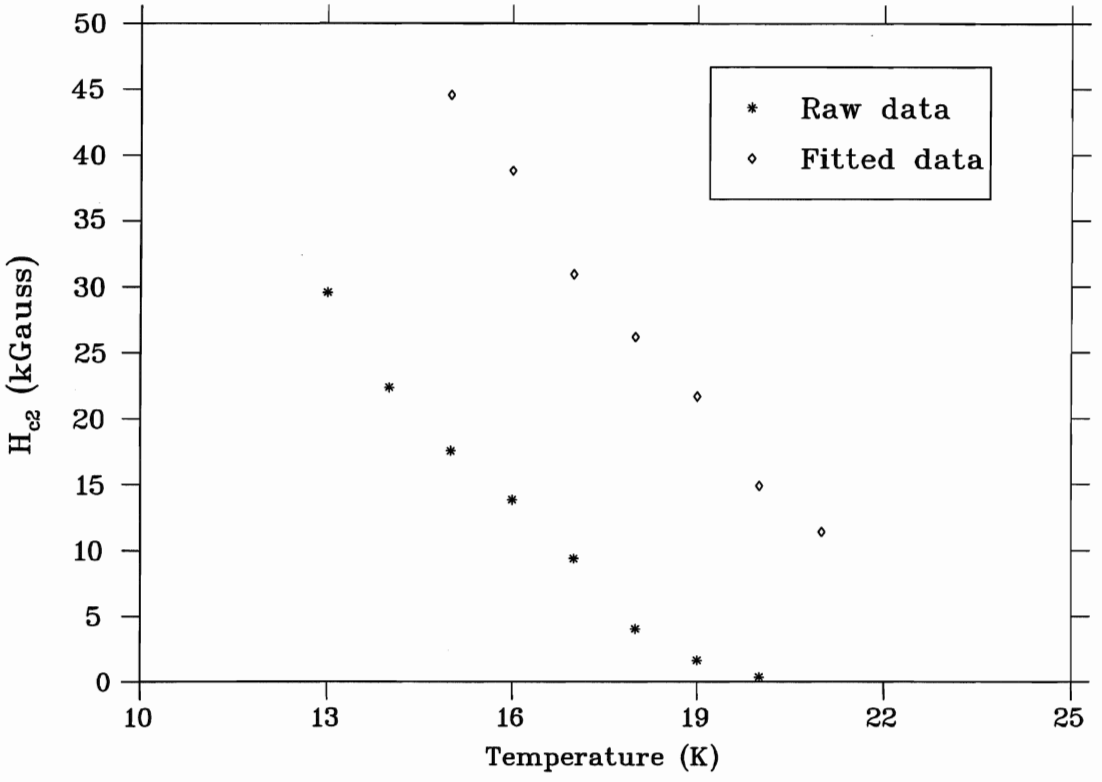

Figure 4.8: **Temperature dependence of H_{c2} as derived from field dependent magnetization measurements**

4.3.2 Temperature dependence of the magnetization

As a complement to field dependence of the magnetization, temperature dependence of the magnetization was also investigated. The magnetization of $YPd_5B_3C_{.3}$ as a function

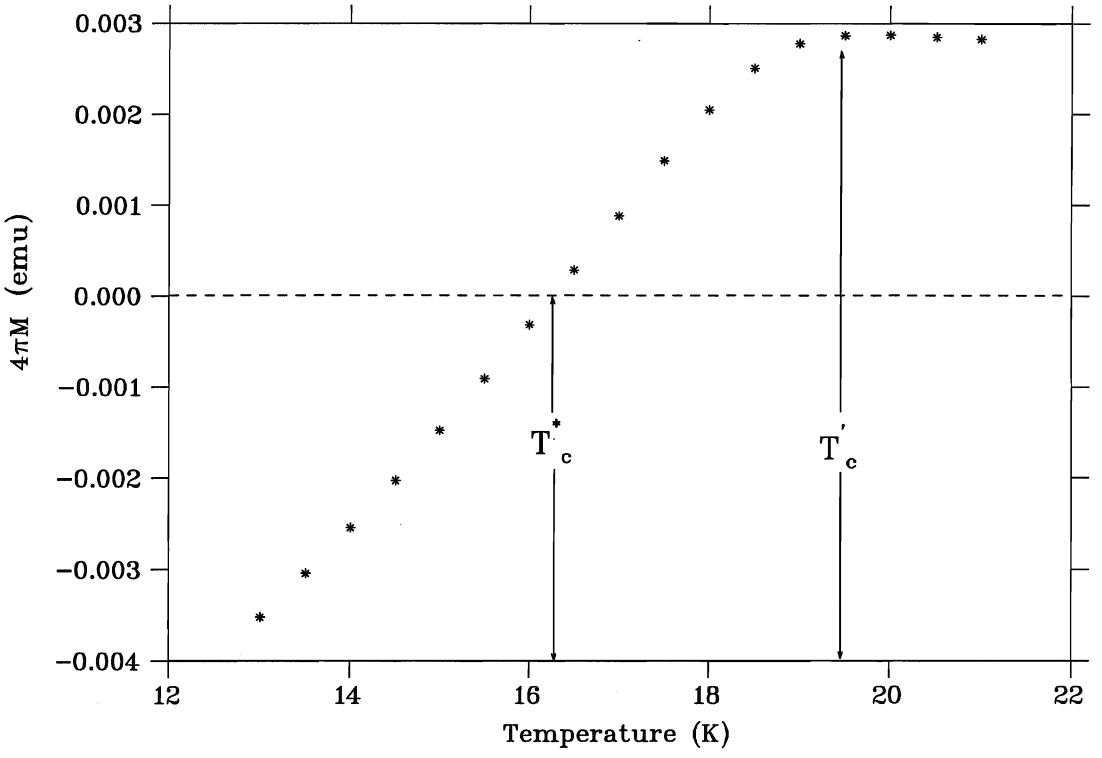

Figure 4.9: **Magnetization of $YPd_5B_3C_{.3}$ as a function of temperature in a field 10000 Gauss**
Note the maximum magnetization occurring at temperature $T_c' > T_c^*$ where traditionally H_{c2} is defined.

of temperature is presented in Figure 4.9 for a field of 1T. H_{c2} is traditionally defined at temperature T^* as shown in the figure. Note the appearance of a slight maximum at temperature T' somewhat greater than T^* Armed with the knowledge that the superconducting volume fraction is small ($\approx 20\%$) compared to the nonsuperconducting volume we now define H_{c2}' at temperature T' as $H_{c2}(T\prime)$. The theoretical magnetization M_{th} at

field B is given by the Ginzburg-Landau theory for the field range $H_{c1} \leq B \leq H_{c2}$ as

$$4\pi M_{th} = -H_{c1} \ln(H_{c2}/B)/\ln \kappa. \tag{4.1}$$

The measured magnetization M_{exp} is divided by M_{th}, and the ratio gives the superconducting volume fraction. The reason for the difference in defining H_{c2} may be explained as a combination of the diamagnetic response of the superconducting volume in our sample and the much larger paramagnetic response of the nonsuperconducting volume. This is a valid assumption provided that the paramagnetic response increases with decreasing temperature in the considered temperature range. As mentioned in the beginning of the chapter, this sample is multiphase and we can be certain only of the existence of the superconducting phase and some other nonsuperconducting phase or phases. If the non-superconducting phase(s) and their corresponding percentage(s) were known it may then be possible to extract the exact temperature dependence of the magnetization provided the following criteria are met:

1. It is possible to synthesize a single phase non-superconducting sample or a two phase sample whose non-superconducting magnetic response is known.

2. The single phase non-superconducting sample has the same magnetic response at a given field as this same phase does in a multiphase sample.

3. It is possible to write $\chi_{dc} = \frac{M}{H}$ in a simple approximation as

$$\chi_{dc} = f\chi_{dia} + (1-f)\chi_{para}, \tag{4.2}$$

where f is the superconducting volume fraction, χ_{dia} is its susceptibility and χ_{para} is the measured susceptibility of the non-superconducting phase [36].

Illustration 4.10 shows the corrected $H_{c2}(T')$ curve. It is important to understand that it is possible that the actual value of H_{c2} occurs at a field other than what we have

defined as $H_{c2}(T\prime)$ however it is certain that the correct value of H_{c2} does not occur where the magnetization goes to zero, defined in this chapter as $H_{c2}(T^{\star})$.

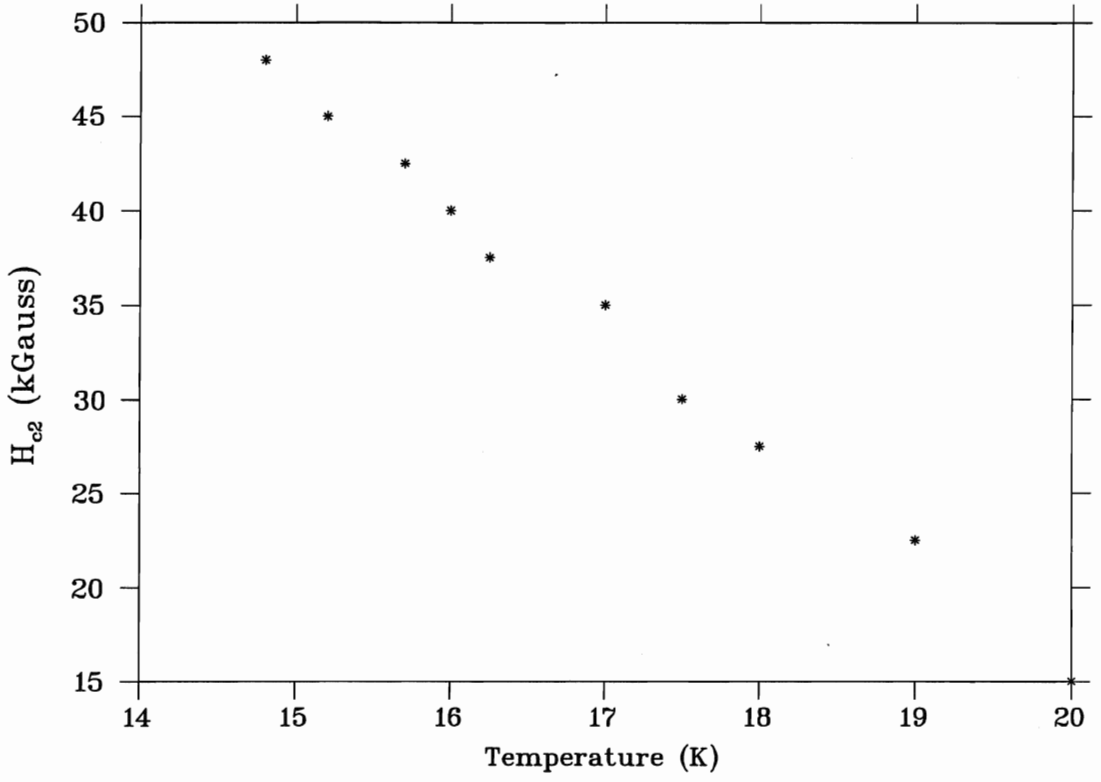

Figure 4.10: **Temperature dependence of H_{c2} as derived from the corrected temperature dependence of the magnetization for $YPd_5B_3C_{.3}$**

Comparison with Figure 4.8 shows that the two methods yield similar $H_{c2}(T)$ phase boundaries.

4.3.3 Magnetoresistance

In an attempt to be certain of the upper critical field phase boundary, magnetoresistive measurements were carried out on the superconducting sample $YPd_5B_3C_{.3}$. Figure 4.11 shows the normalized resistive transition when magnetic fields were applied to the sample

at the temperature intervals T = 21.5, 20, 18, and 16 K. The sample was not removed from the SQUID magnetometer between measurements to ensure that the sample orientation relative to the magnet was unchanged. The results are normalized to the T = 25 K measurements.

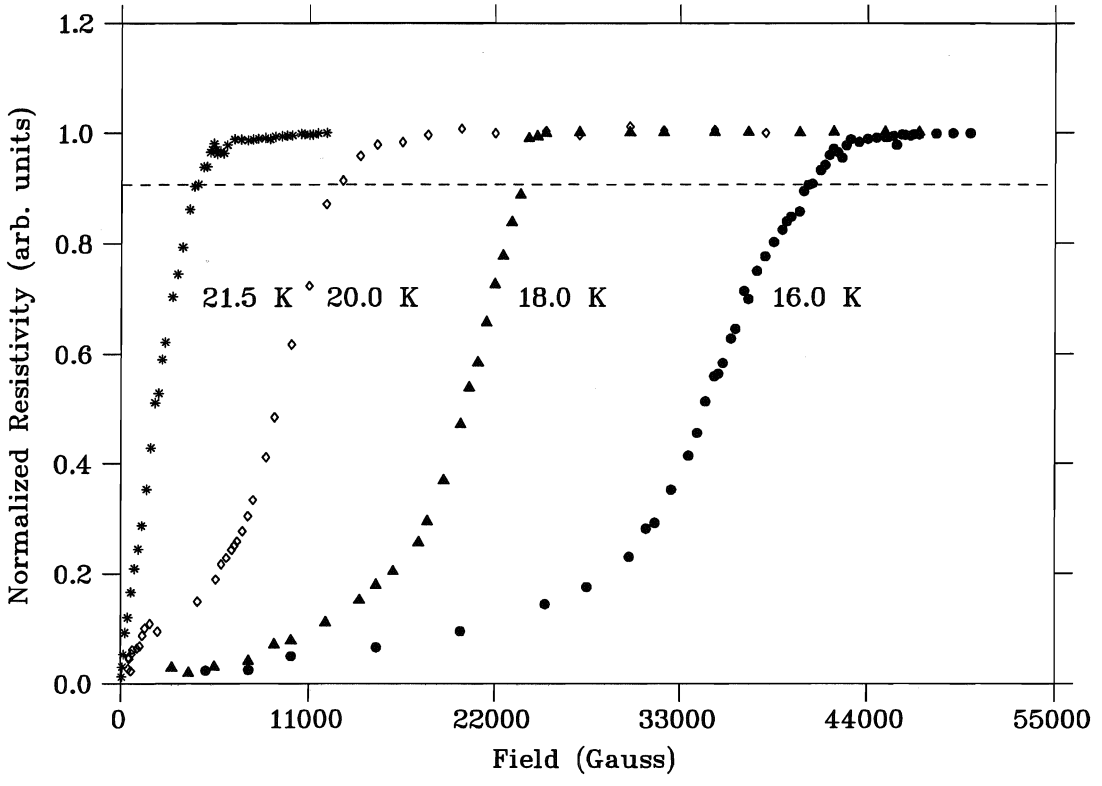

Figure 4.11: **Magnetic field dependence of resistivity for $YPd_5B_3C_{.3}$.** The results were obtained by sweeping the magnetic field while maintaining a constant temperature. Notice the broadening of the transition as the applied magnetic field is increased, most notably in the first 40% of the onset of resistivity. The dashed line represents 90% of the value of normal state resistivity.

It is apparent from Figure 4.11 that the application of a magnetic field alters the onset of superconductivity. At lower temperatures the sample has a much higher value of the upper critical field. As one would expect this is due to surface currents that screen

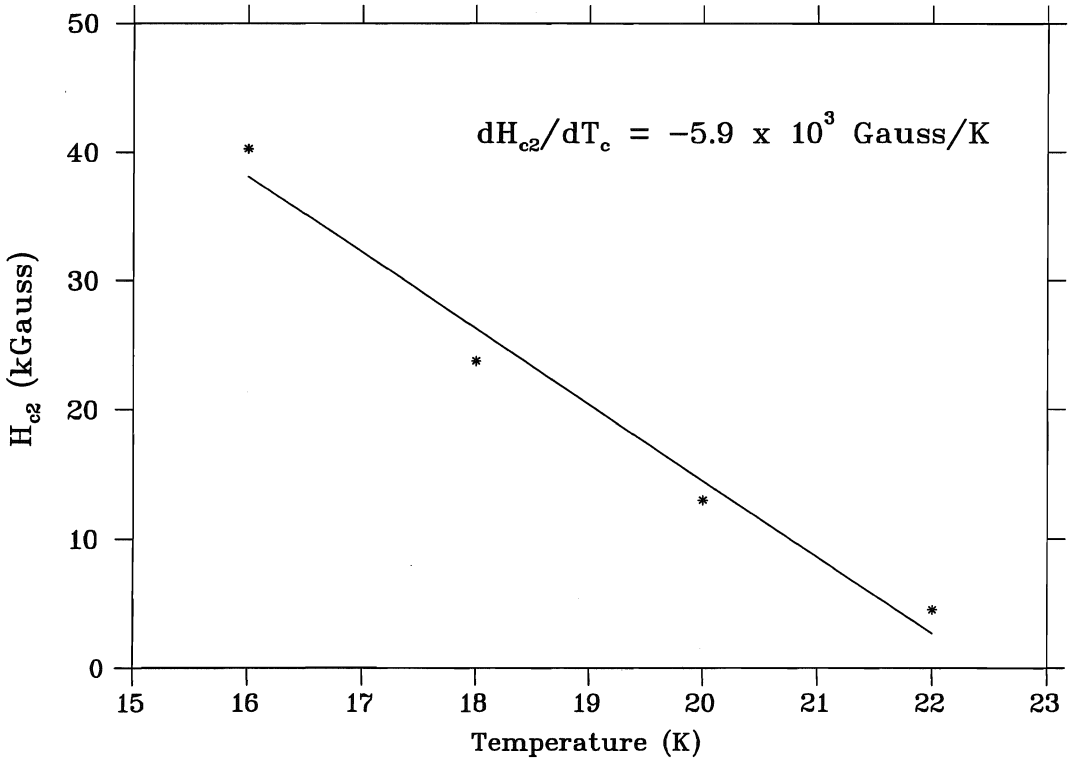

Figure 4.12: H_{c2} **of** $YPd_5B_3C_{.3}$ **as determined by magnetoresistive measurements.**
The data plotted corresponds to 90% of the normal state resistivity. The solid line represents a least squares fit of the data.

the sample and impede the penetration of flux into the sample. The point of interest in the figure is the width of the transition from the superconducting to the normal state. As the temperature is reduced and a magnetic field applied the width of the transition broadens as the magnetic field is increased. Also, this broadening is greatest in the first 40% of the onset of resistance. Above this point the slope of the curves in Figure 4.11 are of the same order of magnitude. This is characteristic of a multiphase sample.

If the value of T_c in Figure 4.11 is taken as 90% of the normal state resistivity, denoted by the dashed line, then the resulting H_{c2} curve appears in Figure 4.12. An

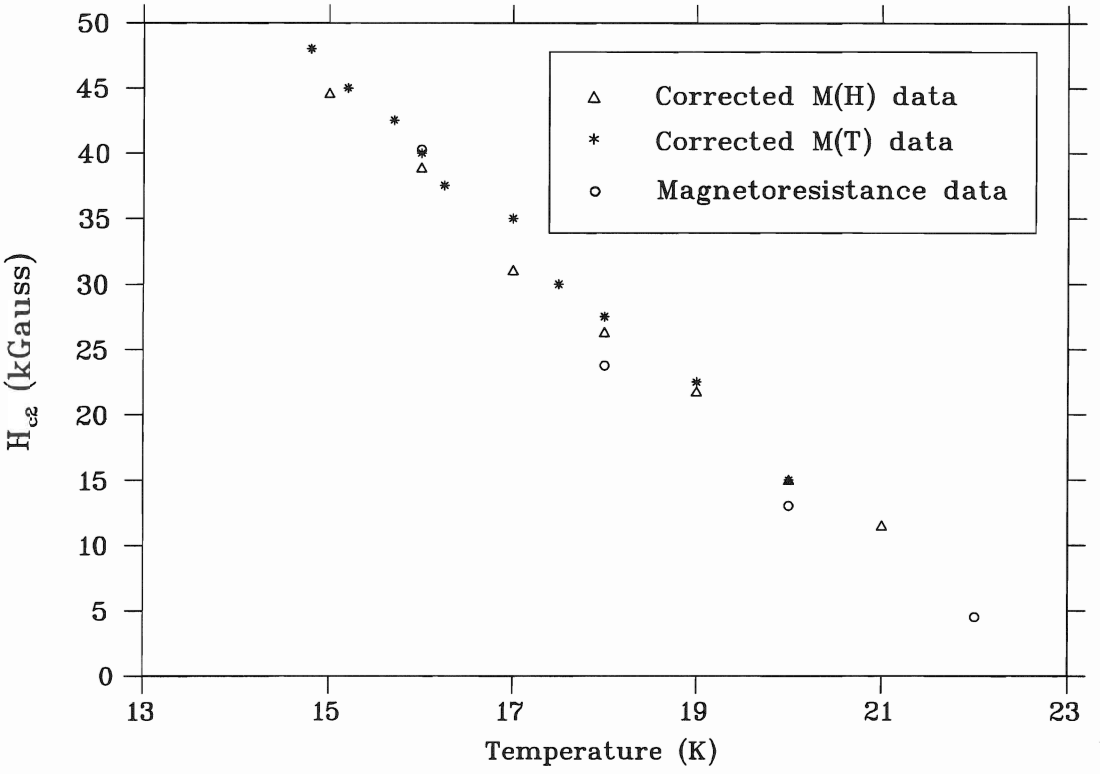

Figure 4.13: **The temperature dependence of** H_{c2} $\triangle$ denotes data acquired from field dependent magnetization experiment, $\star$ represents the result of temperature dependence of the magnetization and the o data were attained using magnetoresistance measurements.

attempt to acquire data at 15 K was unsuccessful. Data accumulation was bound to a lower temperature of 16 K due to limitations of the magnet in the SQUID magnetometer.

Figure 4.13 plots the temperature dependence of the upper critical field as found experimentally by the three means presented in this chapter and offers the reader the opportunity to compare results. By mere inspection it is evident that the three methods produced nearly identical upper critical field phase boundary. Via least squares analysis the slopes, dH_{c2}/dT, of the M(H), M(T) and magnetoresistance derived data were calculated to be $(-5.6 \pm .2) \times 10^3$, $(-6.2 \pm .1) \times 10^3$ and $(-5.9 \pm .6) \times 10^3$ kGauss/K

respectively. An example for the magnetoresistance derived data is shown in Figure 4.12.

From the upper and lower critical field values obtained, several important parameters of the superconducting state can be determined. Using standard expressions for type II superconductors which connect H_{c2} and H_{c1} with the thermodynamic critical field H_c via

$$H_c(T) = \sqrt{H_{c2}(T) \cdot H_{c1}(T)}, \tag{4.3}$$

one can obtain the Ginzburg-Landau parameter using the following equation

$$\kappa = H_{c2}(T)/\sqrt{2}H_c(T). \tag{4.4}$$

In addition the superconducting coherence length ξ was calculated using

$$H_{c2}(T) = \phi_0/2\pi\xi^2(T), \tag{4.5}$$

where ϕ_0 is a constant equal to 2.0678×10^{-7} Gauss $\cdot cm^2$. Table 4.1 lists the results of the calculations.

T_c	22.6 K
$H_{c1}(5K)$	$\sim$ 310 Gauss
$H_{c2}(15K)$	$\sim$ 55000 Gauss
$H_c(15K)$	$\sim$ 3405 Gauss
ξ	$\sim 84\mathring{A}$
κ	$\sim$ 9.5

Table 4.1: Superconducting parameters for $YPd_5B_3C_{.3}$

4.4 Hydrostatic pressure measurements

The electrical resistance of $YPd_5B_3C_{.3}$ was measured as a function of temperature in the range 4–300 K under applied hydrostatic pressure. In all cases, the temperature dependence of the electrical resistivity is near linear in the high temperature range with a slight

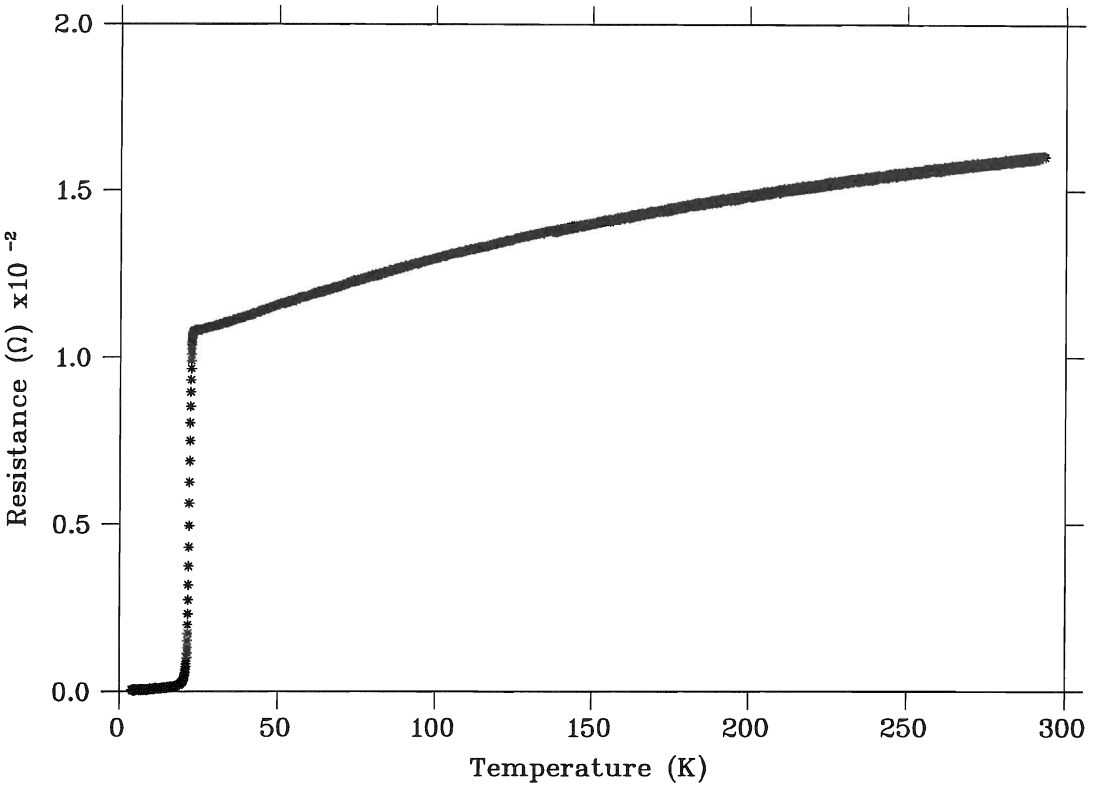

Figure 4.14: **Typical response of the electrical resistance of $YPd_5B_3C_{.3}$ under applied pressure 4 Kbar.**

positive slope, changing drastically only at the onset of superconductivity. Figure 4.14 shows a typical set of data. Measurements were taken on initial cooling and subsequent warming of the pressure apparatus. The transition temperature was taken as the temperature at which the superconducting transition reached 50% of its normal state value. The applied pressure was determined using a standard lead manometer. The pressure dependence of the transition temperature for lead was given in chapter 3. Figure 4.15 shows the response of the superconducting sample $YPd_5B_3C_{.3}$ under a range of applied hydrostatic pressures. There are two trends that appear as the pressure is increased. First the width of the transition temperature decreases as applied pressure is increased.

This is in contrast with the high-T_c cuprate superconductors where their short coherence lengths (typically 20$\mathring{A}$) result in significant broadening of the resistive temperature under pressure. The narrowing of the transition in the Y-Pd-B-C system may be partially explained in the following manner. Since the $YPd_5B_3C_{.3}$ sample is multi–phased and only one of the several possible phases has been found to be superconducting [8] the path of least resistance may have been shortened under applied pressure. Any arbitrary piece of sample will in all likelyhood contain both normal and superconducting regions. Since the volume fraction of this particular sample is $\approx$ 20 % there is a high probability that the superconducting path is very long. The superconducting path is defined to be the shortest distance from one region of superconducting material to another. When the sample is at ambient pressure and in the superconducting temperature range, a current will attempt to travel the path of least resistance (ie. it will travel from one superconducting region to the next). What I am suggesting is that at ambient pressure there is no single path a current may travel without crossing some region of normal material. As pressure is applied the shortest path contains a larger percentage of superconducting material and fewer normal regions. This is not to suggest that the superconducting volume of the sample has changed, merely that the distance from one superconducting region relative to the nearest neighbouring superconducting region has become smaller. As pressure is applied the shape of the superconducting regions has been altered such that some of these regions now overlap each other instead of being isolated from one another by pockets of normal material.

The second and most notable trend is the shift of the superconducting transition to lower temperatures as a function of pressure. It is plausible that there are several mechanisms responsible for this shift in T_c however the scope of this research limits the discussion. The simplest approach is to consider the effect of pressure on T_c according to

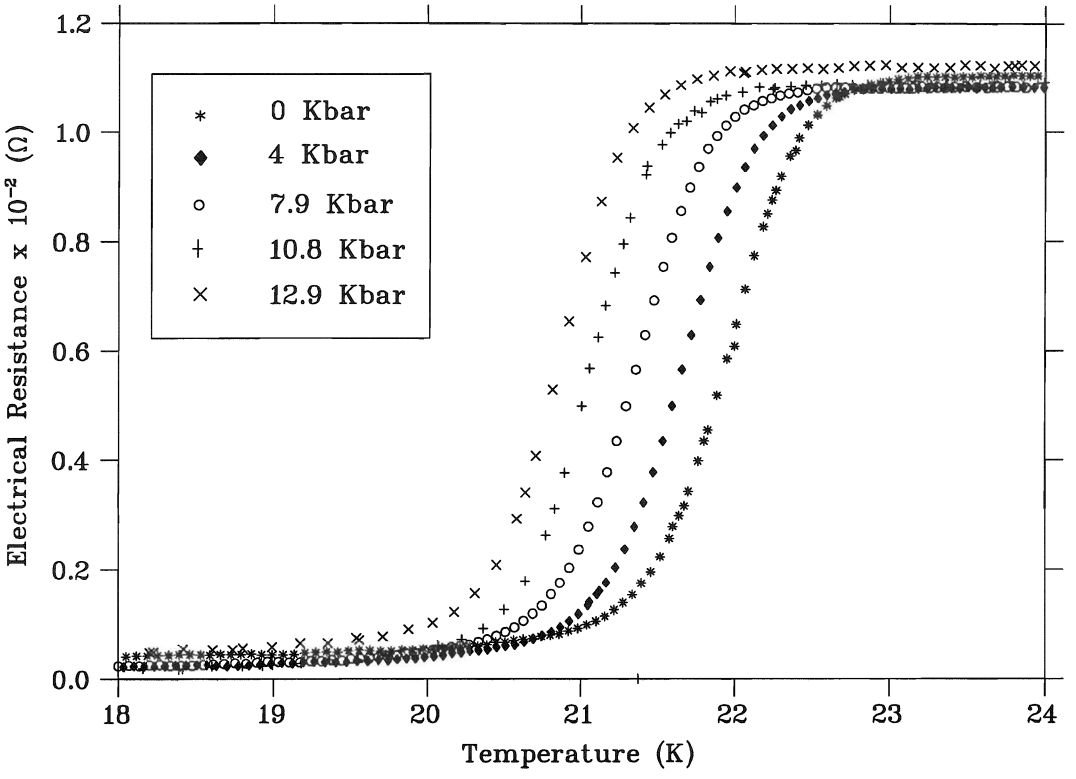

Figure 4.15: **The response of $YPd_5B_3C_{.3}$ under applied hydrostatic pressure.**
There are two items the reader should note. First is the narrowing of the transition temperature as pressure is increased and second, the reduction of the transition temperature as pressure is increased.

the BCS theory as given by equation 2.5 which was:

$$T_c = 1.14\langle\omega\rangle_{ph} exp[-1/N(E_f)V_{BCS}]. \tag{4.6}$$

In principle, a change of T_c may be attributed to either a change in the phonon frequency, variations in V_{BCS} or a change in the density of states. If one considers the atoms of a lattice to be simple harmonic oscillators then, as pressure is increased, the spring constant between the atoms becomes larger (ie. the lattice stiffens) and the frequency of oscillation would increase. In practice, the change of the lattice parameter with applied pressure is of the order $< 1\%$ and, as discussed in section 2.4, an increase in the phonon frequency should be accompanied by an increase in the critical temperature in this simple approximation. However, there are some problems with the BCS theory as also discussed in chapter 2, most notably, the failure to explain the reduction of T_c in systems with flat band structures such as Lead. I will instead turn to the McMillan equation first introduced in chapter 2 to aid in the explanation of $T_c(P)$.

Recall the McMillan equation

$$T_c \sim \langle\omega\rangle_{ph} exp[-M\langle\omega\rangle_{ph}^2/N(E_f)V]. \tag{4.7}$$

The most significant difference between the McMillan and BCS equations appears in the exponential term, more specifically the presence of $\langle\omega\rangle_{ph}^2$ in McMillan's equation. It is this term that allows dT_c/dP of Lead to be negative even though only phonon frequencies are involved in the change of T_c under pressure. While it is true that $\langle\omega\rangle_{ph}$ will increase under applied pressure, causing the first $\langle\omega\rangle_{ph}$ term to increase and attempt to drive T_c to a higher level, it is overridden by the square term in the exponential. Since the exponential is negative, the actual contribution to T_c due to phonon frequencies is the product of the two competing phononic contributions which results in a net loss of T_c under pressure.

Now the role of the electronic density of states must be addressed. The pressure derivative of the critical temperature dT_c/dP of $YPd_5B_3C_{.3}$ is given in Figure 4.16. The value of T_c plotted is the midway point between the 10% and 90% values of the transition in Figure 4.15. Upon inspection, one might initially associate such a small

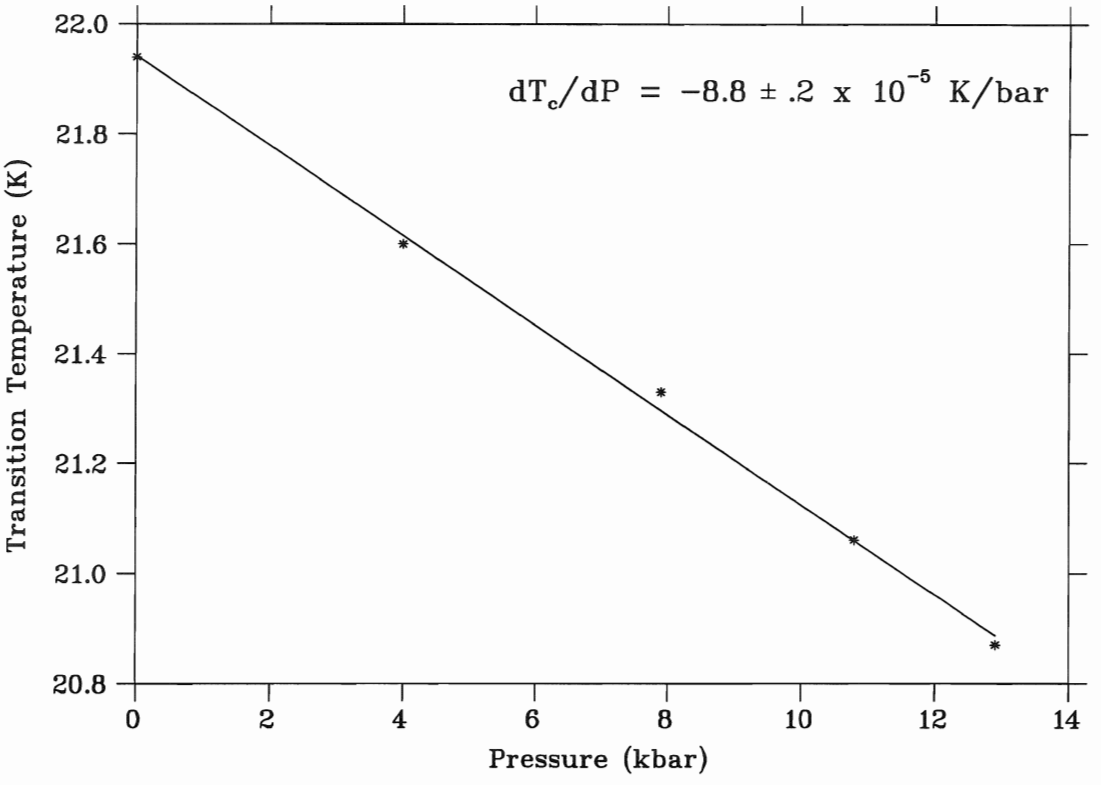

Figure 4.16: **Critical temperature of $YPd_5B_3C_{.3}$ as a function of pressure**
The value used for T_c at each pressure is the midway point between the 10% and 90% values of the transition shown in Figure 4.15

pressure derivative (here $dT_c/\mathrm{dP} \approx 10^{-5}$ K/bar) with a band structure predicted by free electron theory. A nearly constant electronic density of states could account for a small difference in T_c as a large pressure is applied. However, such a band structure is indicative of s band metals while the Y-Pd-B-C system is dominated by the d-band structure of

both Yttrium and Palladium. This suggests that the tight binding model may provide more practical insight into the role of $N(E_f)$. Alternatively, or in addition a $T_c(P)$ effect similar to the one observed in this system could be realized in a model where electronic contributions are important; that is where pressure would force E_f to increasingly lower values of the density of states.

Such is the case in the YNi_2B_2C system. Measurements of T_c as a function of pressure have been performed by Schmidt an Braun [37]. Here, the the pressure dependence of YNi_2B_2C was found to be $\approx -1 \times 10^{-5}$ K/bar, however no mention was made of a possible mechanism. These findings disagree with those of reference [38] where it was reported that dT_c/dP in the Y-Ni system is $\approx +3 \times 10^{-5}$ K/bar. This group suggests that the mechanism responsible for the change in T_c is the competition of electronic and phononic contributions of opposite sign. While the phononic term is expected to be negative due to lattice stiffening (this is the contribution to T_c from $\langle\omega\rangle^2_{ph}$ in the McMillan equation 2.7), the electronic contribution is greater due to a shift in the density of states from the low energy side at the Fermi level to the high energy side.

Band structure calculations [39] show that YNi_2B_2C has a peak in the density of states of predominantly Ni 3d character and that the Fermi level is positioned on the low side near this maximum. Since it has been reported that the superconducting phase of $YPd_5B_3C_{.3}$ is equivalent to that of $LuNi_2B_2C$, where Y is substituted for Lu and Pd for Ni [12], it seems safe to suggest that the band structure of the superconducting phase YPd_2BC is similar to that of YNi_2B_2C. Figure 4.17 is a schematic drawing of the proposed density of states for the superconducting phase YPd_2BC as calculated by Coehoorn [40]. Calculations were done from first principles using the augmented spherical wave method. The author suggests that the superconductivity of the Y-Pd system is related to the presence of a narrow peak in the density of states at the Fermi level, which appears as the dotted line in Figure 4.17.

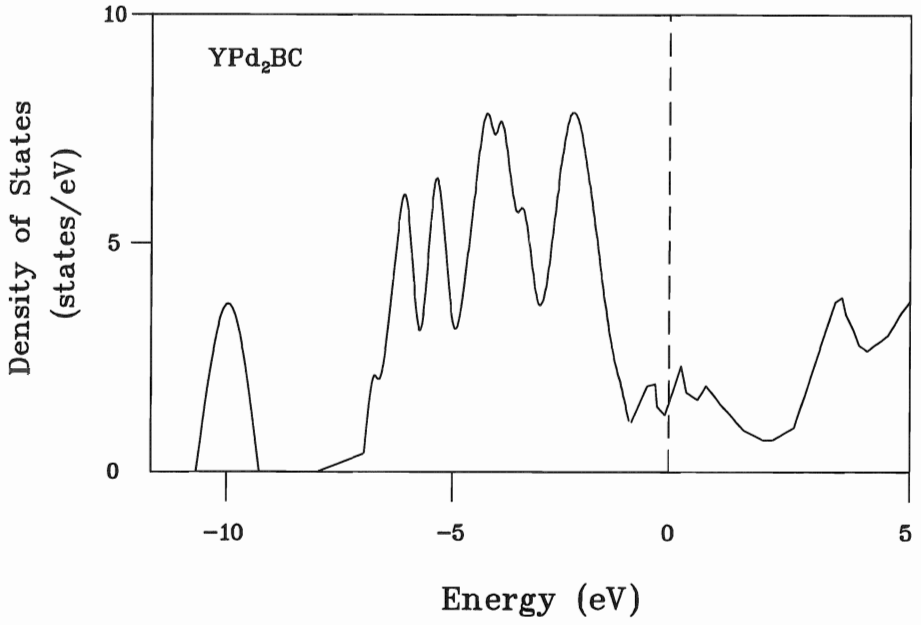

Figure 4.17: **Schematic drawing of the proposed density of states for YPd_2BC**
Notice the Fermi level lies very close to a peak in the density of states. Application of external pressure would force the density of states to the high side of the peak. The dotted line represents the location of the Fermi level. (Adapted after [40]).

Based on the pressure derivatives of Lead ($dT_c/dP \sim -10^{-3}$), the contrasting reports for the Y-Ni system which were $dT_c/dP \sim -10^{-5}$ and $dT_c/dP \sim +3 \times 10^{-5}$ according to references [37] and [38] respectively along with the findings of this study ($dT_c/dP \sim -10^{-5}$ for the Y-Pd-B-C system), some explanations are possible. The possibility exists that within experimental error there is in fact no change in T_c under pressure in either the Y-Ni or Y-Pd systems if one bases their hypothesis on the basis of the orders of magnitude involved. When compared with the change in T_c of lead under pressure, Y-Ni and Y-Pd experience only one percent losses in their transition temperatures, for all intents and purpose this may be considered as no loss at all, however considering the

conflicting reports as to whether T_c is either enhanced or reduced in the Y-Ni system under pressure, it is more likely that the effect is sample dependent. Considering the similarity in both crystal and electronic structure of the Y-Ni and Y-Pd systems, this may also be true in the mixed phase sample $YPd_5B_3C_{.3}$. Finally, it seems evident that there may be more than one mechanism responsible for the change in T_c under pressure. The most likely scenario is the competition between the enhancement of T_c from the linear $\langle\omega\rangle_{ph}$ factor and more importantly from the shift in the electronic density of states to the high side of a peak at the Fermi level, with the simultaneous reduction in T_c by the square of the average phonon frequency in the exponential of the McMillan equation which in fact dominates and results in the lowering of T_c under external pressure in the Y-Pd-B-C system.

Chapter 5

Conclusions

The macroscopic magnetic properties of the superconducting phase of Y-Pd-B-C have been determined and analyzed. The onset of superconductivity was observed at 22.6 K with zero resistance occurring at at 21.2 K. Superconducting parameters H_{c1}, H_{c2}, ξ and κ have been estimated. The compound appears to be an extreme type II superconductor with $\kappa > 9$, and $\xi \approx 80\mathring{A}$, both of which are in good agreement with [10]. The critical fields H_{c1} and H_{c2} were determined to be approximately to be 310 Gauss and > 55000 Gauss at 5 K and 15 K respectively.

The behavior of $T_c(P)$ for $YPd_5B_3C_{.3}$ was discussed in terms of the competition of phononic and electronic contributions of opposite signs. The density of states at the Fermi level is according to band structure calculations expected to shift from the low side to the high energy side of a peak, while the phonon frequency increases and is the dominant force driving the transition to lower temperatures under applied pressures. $T_c(P)$ was found to decrease linearly with $dT_c/dP \approx -8.8 \times 10^{-5} K/bar$. Further measurements of the influence of pressure on the phonon spectrum and the effect of composition on dT_c/dP are required for a complete analysis of the influence of pressure on the individual parameters in the equation for T_c.

Clearly the next step required in the study of this compound involves concentrated effort to synthesize single phase, superconducting samples. Once this process has been perfected, then research may continue in hope of devising methods to enhance T_c.

Bibliography

[1] J.G. Bednorz and K.A. *Müller*, Z.Phys. B **64**, 189, (1986).

[2] C.W. Chu, P.H. Hor, R.L. Meng, L. Gao, Z.G. Huang, and Y.Q. Wang, Phys. Rev. Letters, **58**, 405, (1987).

[3] M.K. Wu, J.R. Ashburn, C.J. Torng, P.H. Hor, R.L. Meng, L. Gao, Z.J. Huang, Y.Q. Wang, and C.W. Chu, Phys. Rev. Letters **58**, 908, (1987).

[4] J. Akimitsu, A. Yamazaki, H. Sawa, and H. Fujiki, Japanese Journal of Applied Physics **26**, 2080, (1988).

[5] A. Schilling, M. Cantoni. J.D. Guo, and H.R. Ott, Nature **363**, 56 (1993).

[6] D.C. Johnston, Solid State Communications **24**, 699, (1977).

[7] B.W. Roberts, Journal of Physical and Chemical Reference Data **5**, 581, (1976).

[8] C. Mazumdar, R. Nagarajan, C. Godart, L.C. Gupta, S.K. Dhar, C. Levy-Clement, B.D. Padalia, and R. Vijayaraghavan, Solid State Communications **87**, 413, (1993).

[9] R.J. Cava, H. Takagi, B. Batlogg, H.W. Zandbergen, J.J Krajewski, W.F Peck Jr, R.B van Dover, R.J. Felder, T. Siegrist, K. Mizahashi, J.O. Lee, H. Eisaki, S.A. Cater, S. Uchida, Nature **367**, 146, (1994).

[10] Y.Y. Xue, Y. Cao, R.L. Meng, C. Kinalidis and C.W. Chu, Physica C **227**, 63, (1994).

[11] H.W. Zandbergen, W.G. Sloof, R.J. Cava, J.J Krajewski, W.F Peck Jr, Physica C **226**, 365, (1994).

[12] C.L. Jia, Y.H. Xu, M. Beyss, F. Peter, and K. Urban Physica C **229**, 325, (1994).

[13] D.D Lawrie, J.P. Franck, Physica C **245**, 159, (1995).

[14] L.F. Mattheiss, T. Siegrist, and R.J. Cava, Solid State Communications **91**, 587, (1994).

[15] A.C. Rose Innes and E.H. Rhoderick, *Introduction to Superconductivity* (Pergamon Press, Toronto, 1978).

[16] M. Reedyk, Ph.D. Thesis, McMaster University, 1992.

[17] Bernard Serin in *Superconductivity volume 2*, edited by Robert Parks (Marcel Dekker, Inc., New York, 1969.).

[18] Charles Kittel, *Introduction to Solid State Physics Sixth Edition* (John Wiley and Sons, Inc, New York, 1986).

[19] Gerald Burns, *An introduction to high temperature superconductivity* (Academic Press Inc, New York, 1992).

[20] D. Cribier, B. Jacrot, L. Madhoz Rao, B. Farnoux, Physics Review **9**,106 (1964).

[21] T.F. Smith, Journal of Low Temperature Physics **6**, 171, (1972).

[22] T. Miyatake, S. Goth, N. Koshizuka, and S. Tanaka, Nature**341**, 41 (1989).

[23] J.S. Schilling, S. Klotz, in The Influence of High Pressure on the Superconducting and normal properties of High Temperature Superconductors, *Physical properties*

of high temperature superconductors III, edited by D.M. Ginsberg (World Scientific, 1992).

[24] J.Karpinski, E. Kaldis, E. Jilek, S. Rusiecki, and B. Bucher, Nature **336**, 660 (1988).

[25] H.Takagi, R.J. Cava, H. Eisaki, J.O. Lee, K. Mizahashi, B. Batlogg, S. Uchida, J.J Krajewski, and W.F. Peck Jr, Physica C **228**, 389, (1994).

[26] J. Bardeen, L.N. Cooper, J.R. Schrieffer, Physical Review **106**, 162 (1957).

[27] W.L. McMillan, Physical Review **167**, 331, (1968).

[28] N.W. Ashcroft, D.N. Mermin, *Solid State Physics* (Holt, Rienhart and Winston, Philadelphia, 1976).

[29] G.Gladstone, M.A. Jensen, J.R. Schrieffer in *Superconductivity volume 2*, edited by Robert Parks (Marcel Dekker, Inc., New York, 1969).

[30] Quantum Design, *Magnetic Property Measurement System Software Manual* (Quantum Design Inc, 1990).

[31] F. Hamed, M.Sc. Thesis, Brock University, 1991.

[32] A. Eichler, J. Witting and Z. Angew, Physica **25** , 319 (1968).

[33] Lakeshore Cryotronics, *Lakeshore Cryotronics Instruction Manual* (Lakeshore Inc, New York, 1988).

[34] R.J. Cava, H. Takagi, H.W. Zandbergen, J.J Krajewski, W.F. Peck Jr, T. Siegrist, B. Batlogg, R.B. Van Dover, R.J. Felder, K. Mizahashi, J.O. Lee, H. Eisaki, and S. Uchida, Nature **367**, 252, (1994).

[35] D.T. Adroja, B.D. Rainford, A.V. Volkozub, P.A.J de Groot, Physica C **229**, 193, (1994).

[36] P.N. Arberg, F.S. Razavi, F.P. Koffyberg, B. *Mitrović*, Solid State Communications, **65**, 849, (1988).

[37] H. Schmidt, and H.F. Braun, Physica C **239**, 315, (1994).

[38] E. Alleno, J.J. Neumeir, J.D. Thompson, P.C. Canfield, and B.K. Cho, Physica C **242**, 169, (1994).

[39] L.F. Mattheiss, Phys.Rev.B **49** (1994).

[40] R. Coehoorn, Physica C **228**, 331, (1994).